IS THERE A LOCAL GREEN DIVIDEND? EVIDENCE FROM INDUSTRIAL SHUTDOWNS IN GERMANY

PHILIPP BOTHE

WORKING PAPER N°2024/22

UPDATED VERSION
AUGUST 2026

WORLD INEQUALITY LAB

Is There a Local Green Dividend? Evidence from Industrial Shutdowns in Germany

Philipp Bothe*
Paris School of Economics

August 2026

Abstract

Large industrial facilities are both sources of pollution and anchors of local labor demand. I construct a 1 km × 1 km panel that links 345 facility shutdowns to environmental and socioeconomic outcomes in Germany over 2010–2021. Exploiting the staggered timing of closures, the empirical design compares neighborhoods around earlier-closing plants to those around later-closing plants. Closures improve local air quality, with gains concentrated in low-income neighborhoods that also bear the largest baseline exposure burden. Nonetheless, housing prices fall by 1.6% on average and by 3.1% three years after closure. This decline coincides with a deterioration in local labor markets. Where industrial employment is high at baseline, average disposable household income falls by almost 2% and unemployment rises significantly. Embedding these estimates in a Rosen-Roback framework recovers a decline in non-market amenities in precisely those places. The removal of a local pollution source does not automatically generate a "green dividend".

JEL Codes: J65, Q51, Q52, Q53, R23, R31

Keywords: Air Pollution, Environmental Inequality, Housing Markets, Industrial Shutdowns, Local Labor Markets, Spatial Equilibrium

---

*Paris School of Economics & EHESS, philipp.bothe@psemail.eu, 48 boulevard Jourdan, 75014 Paris. I am grateful to Thomas Bezy, Lucas Chancel, Ignacio Flores, Marc Fleurbaey, Meredith Fowlie, Gordon Hanson, Emmanuelle Lavaine, Cornelia Mohren, Thomas Piketty, Ed Rubin, Lutz Sager, Gregor Singer, Constanza Tomaselli, Randall Walsh, Paige Weber, and Yanos Zylberberg for helpful comments and suggestions. Earlier versions of this paper circulated under the title "Lost in Aggregation: The Local Environmental and Welfare Effects of Large Industrial Shutdowns". This work was funded by a French government subsidy managed by the Agence Nationale de la Recherche (ANR) under the framework of the "Investissements d'avenir programme" reference ANR-17-EURE-001 and by the European Union under WISE Horizons Grant No. 101095219.

I INTRODUCTION

The removal of a local pollution source is commonly presumed to yield a net gain in residential desirability for surrounding neighborhoods. The intuition is straightforward. When a major source of environmental disamenity is removed, surrounding neighborhoods become more desirable places to live, and the resulting capitalization should appear in housing prices. A substantial body of US-based evidence supports this view. Studies of toxic plant openings and closings (Currie et al., 2015), hazardous waste and brownfield cleanups (Linn, 2013; Gamper-Rabindran and Timmins, 2013; Haninger et al., 2017), and most recently coal-fired power plant retirements (Fraenkel et al., 2024) consistently document positive housing price responses to the removal of local pollution sources.[1] Mirroring these findings, Davis (2011) documents negative effects of power plant openings on nearby housing values and rents while Muehlenbachs et al. (2015) show that property values decline for groundwater-dependent homes following shale gas development. These findings are consistent with the hypothesis of a local "green dividend", i.e., the idea that removing a pollution source delivers a net welfare gain to the host community through capitalized amenity improvements. A broader literature documents positive capitalization of air quality improvements more generally (Chay and Greenstone, 2005; Grainger, 2012; Freeman et al., 2019; Graff Zivin and Singer, 2022; Sager and Singer, 2025).

This paper argues that shutting down polluting industrial sites does not automatically generate such positive net effects on residential desirability. Whether a shutdown leaves a host community better or worse off overall depends on how two opposing forces net out. A closure plausibly induces an improvement in local environmental quality and an adverse labor demand shock at the same time. Where the closure removes a pollution source but local labor demand is largely unaffected, the air quality gain is not offset by any countervailing shock, and capitalization is expected to be positive. But when the same facility also represents an important component of local labor demand, the labor demand shock can outweigh the gain in air quality. Moreover, the exit of a major local employer can erode other dimensions of local desirability such as public services or retail so that the overall change in non-market amenities may be negative even as environmental quality improves.

This ambiguity follows directly from standard spatial equilibrium logic (Bayer et al., 2016;

[1] In contrast, Greenstone and Gallagher (2008) find no capitalization effect of Superfund cleanup at the census-tract level.

Balboni and Shapiro, 2025). A shutdown shifts both the amenity and the income argument of the location choice problem, in opposite directions. Which channel dominates is an empirical question, and one whose answer plausibly varies with the local economy's reliance on industrial activity. Recent evidence from the US coal transition is consistent with this conditionality. Fraenkel et al. (2024) explicitly show that the coal unit retirements in their sample (which they find to have positive housing price effects) have negligible local employment effects. Where shutdowns coincide with substantial earnings losses for displaced workers and broader regional decline (Hanson, 2023; Colmer et al., 2024; Krause, 2026b), the conditions for a local "green dividend" may not hold.

Germany provides a useful setting for studying these conditions. Ongoing deindustrialization (Gornig and Goebel, 2018) and the staged phase-out of nuclear and coal power (Bauer et al., 2017; Bruns and Thomsen, 2025) have produced numerous closures of large industrial facilities, many of them in regions where the affected sites are central to the local employment base, such as the Ruhr Area in West Germany. Worker-level evidence confirms that displacement from carbon-intensive industries generates persistent earnings scars (Barreto et al., 2023; Colmer et al., 2024; Haywood et al., 2024; Rud et al., 2024). Closest to this paper, Bauer et al. (2017) show that housing values decline after the post-Fukushima closure of German nuclear power plants and provide municipality-level evidence consistent with adverse local economic effects dominating any amenity gain from perceived nuclear risk reductions. This paper extends the existing evidence by estimating this trade-off at the localized level at which it plausibly materializes (vom Berge and Schmillen, 2023) and by generalizing the results to a significantly broader set of industrial shutdowns.

In this paper, I construct a novel panel that links information on industrial facility shutdowns with data on air quality, socioeconomic outcomes, and housing prices at the 1km $\times$ 1km neighborhood level for all populated areas of Germany over 2010–2021. The closure data are drawn from the EU Industrial Reporting Database (IRD), which records the operational status of large polluting facilities and allows me to identify 345 distinct plants that transition from functional to decommissioned or disused during the period 2017–2021.[2] I exploit the staggered timing of these closures within an event study framework that compares grid cells that experience a shutdown in a given year to grid cells that will experience a shutdown later during the observation period. By restricting the sample to neighborhoods within a fixed radius

[2]Operational status is recorded from 2016 onward, so that the first change in operational status which I use to define a shutdown can occur in 2017.

of facilities that close at some point during the observation window, identification comes from differences in closure timing rather than from differences in industrial siting across space.

The empirical results document a clear trade-off. Closures generate moderate but statistically significant improvements in local air quality, with PM2.5 reductions concentrated in lower-income neighborhoods that bear a disproportionate pollution burden at baseline. In this dimension, IRD shutdowns deliver the environmental amenity gains that the existing literature would predict. Yet housing prices decline rather than appreciate, falling by approximately 3.1% at the end of the event window. This price decline coincides with a deterioration of local labor market conditions. Average disposable household income per adult falls and unemployment rises in affected neighborhoods, while population does not appear to respond significantly.[3] Additionally, there is pronounced heterogeneity in this pattern. In neighborhoods located in districts with high baseline industrial employment shares, the income loss more than doubles relative to less industrial areas and unemployment rises by an additional 0.5 percentage points.

I embed the reduced-form estimates in a Rosen-Roback location choice framework adapted from Bartik et al. (2019). The framework allows me to back out the residual non-market amenity component of location value implied by observed changes in income, housing prices, and population. In high-industrial neighborhoods, this residual deteriorates following a closure, indicating that the air quality improvement is more than offset by losses along other dimensions of local quality consistent with broader patterns of regional decline (Gagliardi et al., 2023; Krause, 2026b). The absence of a population response in these neighborhoods is reconciled in the model through the housing price decline itself, which compensates for the loss in nominal income. Yet, from a place-based perspective, the post-closure bundle of amenities, housing prices and wages constitutes a short-term decline rather than a net welfare gain.

This paper makes two contributions. The primary contribution is to show that the local green dividend is conditional and requires that a closure remove a pollution source without simultaneously delivering a substantial shock to local labor demand. In the German industrial closures I study, this condition fails more often than not. Labor market losses accompany the doc-

[3] Note that the absence of a significant population response might be due to the relatively short post-treatment window. A longer horizon might be needed to capture compositional changes that environmental amenity shocks have been shown to introduce (Banzhaf and Walsh, 2008; Gamper-Rabindran and Timmins, 2011; Depro et al., 2015; Coulomb and Zylberberg, 2021; Heblich et al., 2021).

umented improvements in environmental quality and dominate the housing market response. This is especially true in industrially dependent regions, where the recovered amenity index shows that improved environmental quality is more than offset by deterioration along other dimensions of local desirability. The secondary contribution is descriptive. Using 1km $\times$ 1km grid-cell panel data covering all populated areas of Germany over 2010–2021, I document a persistent PM2.5 exposure gap of 0.25 standard deviations across the neighborhood-level income distribution. This is, to my knowledge, the most granular longitudinal estimate of exposure inequality in Germany to date, adding to the evidence on disproportionate environmental burdens borne by economically deprived and non-white communities (Mohai et al., 2009; Miranda et al., 2011; Bell and Ebisu, 2012; Ash and Boyce, 2018; Rüttenauer, 2018; Jbaily et al., 2022). I further show that closures themselves narrow this gap, consistent with the progressive incidence of environmental amenity gains documented in the US (Colmer et al., 2020; Currie et al., 2023).

These results have implications for the political economy of the green transition. Industrial and decarbonization policies are typically designed and evaluated at an aggregate level, but their welfare consequences are heterogeneously distributed across locations. In neighborhoods where industrial employment is concentrated, structural change can exacerbate local inequality even when it delivers genuine environmental benefits. This suggests that environmental mandates likely require complementary place-based economic policies to prevent regional decline in the most exposed areas (Hanson, 2023; Krause, 2026a).

II DATA

The empirical analysis combines data on neighborhood-level socioeconomic conditions, residential real estate listings, satellite- and monitor-based measures of ambient air pollution, reanalysis data on local weather, and administrative records on the location and operational status of industrial facilities in Germany. All variables are aggregated to the annual level and matched onto a common 1 km $\times$ 1 km grid covering the populated area of Germany over the period 2010–2021. The remainder of this section describes each source and how it is matched onto the reference grid.

SOCIOECONOMIC DATA

Socioeconomic data at the grid cell level are obtained from RWI-GEO-GRID, provided by the Research Data Center at *RWI – Leibniz Institute for Economic Research* (Breidenbach and Eilers, 2018). The underlying microdata are compiled from administrative records, commercial address and geomarketing sources, and postal address data, and comprise over one billion individual records. The grid follows the EU-INSPIRE projection, which standardizes spatial referencing across the EU, and partitions Germany into more than 300,000 cells. RWI distributes the data as a scientific use file, with cell-year observations suppressed where fewer than five households reside in a given cell (RWI and Microm, 2023). Retaining cells that are populated and unsuppressed throughout the sample period yields a panel of approximately 150,000 grid cells.

The data describe the residential and demographic structure of each cell, including total population and age composition. They further contain the local unemployment rate and a modeled estimate of total disposable household income per grid cell, which comprises labor and capital income net of taxes and social contributions and includes social transfers received. Dividing total income per cell by the number of residents aged 18 and above, obtained from the cell's age composition, yields average disposable household income *per adult*, which serves as the primary income variable in the analysis.

I complement the grid cell data with district-level information on industrial employment from INKAR, the spatial monitoring database of the *Federal Institute for Research on Building, Urban Affairs and Spatial Development* (Bundesinstitut für Bau-, Stadt- und Raumforschung (BBSR), 2025). The indicator measures industrial employees at place of residence as a share of the working-age population, and is observed for Germany's 401 districts (*Kreise und kreisfreie Städte*). This measure is applied to classify neighborhoods by their pre-closure dependence on industrial employment.

REAL ESTATE DATA

Real estate data (RWI-GEO-RED) are also obtained from the Research Data Center of RWI (Schaffner and Thiel, 2024). The dataset is constructed from listings on *Immobilienscout24*, Germany's largest online real estate platform, and contains detailed property-level information, including listing prices, rents, and dwelling characteristics such as construction year, number of rooms, living space, and plot size. The data cover the period 2007–2022 and are geolocated on the same 1 km $\times$ 1 km grid used for the socioeconomic variables.

Before aggregating to the grid cell level, I impose several sample restrictions on the raw property-level observations.[4] For the rental market, I restrict the sample to apartments with a monthly cold rent (*Kaltmiete*) between €50 and €5,000, a living area between 10 m^2 and 400 m^2, and no more than eight rooms. For house sales, I retain properties with a listing price between €10,000 and €10,000,000, a living area between 25 m^2 and 500 m^2, a plot size of at least 50 m^2, and no more than eleven rooms. For both subsamples, I exclude buildings constructed prior to 1900. I then aggregate to the grid cell level by computing the average listing price per square meter for houses and the average cold rent per square meter for apartments in each cell-year. After imposing these restrictions, 83.5% of cells have at least one house listed for sale across the sample period and 69.9% have at least one apartment listing. Among cells with at least one listing, the average cell has 59 houses and 256 apartments listed across the full observation period. To account for potential composition effects in the housing stock listed for sale or rent, Appendix F reproduces the main results using raw property-level listings with hedonic controls.

Two caveats apply. First, the data reflect listings from a single platform. However, *Immobilienscout24* is the largest real estate platform in Germany (Bundeskartellamt, 2015), and because properties are frequently cross-listed and the site is used by both private homeowners and professional agents, the dataset is likely to capture the vast majority of the online market. Second, the dataset reports listing rather than transaction prices. Henger and Voigtländer (2014) document an average gap of 6.7% between listing and transaction prices for residential properties in Hamburg, suggesting a systematic wedge in levels. Constant place-specific differences in this wedge across regions are absorbed by the granular spatial fixed effects in the empirical application, so that the remaining concern is *differential trends in the listing-transaction price gap* across regions. This cannot be tested without final sales prices, but since sellers facing nominal losses set asking prices well above what they ultimately realize (Genesove and Mayer, 2001), a closure that depresses local property values should attenuate rather than inflate the estimated price declines, if anything.

[4] These restrictions closely resemble those in Bruns and Thomsen (2025).

AIR POLLUTION DATA

Air quality data are drawn from two sources that jointly capture both the fine and the coarse fraction of ambient particulate matter. The first is the global satellite-derived PM2.5 product of van Donkelaar et al. (2021), which combines aerosol optical depth retrievals from multiple satellite instruments with the GEOS-Chem chemical transport model, calibrated against ground-based monitor measurements. The resulting dataset provides annual mean PM2.5 concentrations at $0.01^\circ \times 0.01^\circ$ resolution (approximately 1 km $\times$ 1 km) with global coverage. The second source is provided by the German Federal Environment Agency (UBA) and measures ambient PM10 concentration (Umweltbundesamt, 2023).[5] These data combine hourly readings from a dense network of ground-level monitors with a chemical transport model (*REM-CALGRID*) to produce a gridded dataset at approximately 2 km $\times$ 2 km resolution covering the entire territory of Germany.

The two measures are complementary along two dimensions. The first is the particle size fraction they capture. PM2.5 comprises fine particles below 2.5 μm in diameter, which originate predominantly from combustion processes and from the atmospheric formation of secondary particulate matter downwind of precursor emissions. PM10 additionally includes the coarse fraction between 2.5 and 10 μm, which is generated mechanically through crushing, grinding, the handling of raw materials, and the resuspension of dust from surfaces and roads. This distinction matters here because the coarse fraction is predominantly primary (U.S. Environmental Protection Agency, 2019). It is released as particulate matter by the industrial process itself rather than formed in the atmosphere from gaseous precursors. Movements in coarse particle concentrations are therefore more directly attributable to the activity of a specific nearby facility, whereas an appreciable share of ambient PM2.5 originates in secondary formation from precursors emitted at considerable distance. Since the estimation sample contains many facilities whose particulate releases are dominated by fugitive and process dust rather than stack combustion (Table A.2), the PM10 measure captures a component of their emissions profile to which the satellite PM2.5 product is comparatively insensitive. The second dimension is measurement methodology. The monitor-based PM10 data are anchored in ground-level measurements, with the chemical transport model serving to interpolate between stations. Their reliability therefore declines with distance to the nearest monitor, particularly in rural areas, and the product is reported at a coarser resolution than the satellite product. The

[5] Provided as part of *Umweltbundesamt, Daten der Messnetze der Länder und des Umweltbundesamtes*. Last accessed May 20, 2025.

satellite-based PM2.5 estimates, in contrast, achieve finer resolution and uniform coverage but have been shown to be measured with non-classical prediction error (Fowlie et al., 2019). Using both measures throughout the analysis thus captures air quality impacts across the full particle size distribution while guarding against results that are an artifact of a single measurement approach. Note, however, that since the two outcomes differ in both the pollutant measured and the underlying measurement technology, differences between the corresponding estimates reflect both margins jointly and are interpreted with this caveat in mind.

For both measures, I compute average annual exposure at the grid cell level as the area-weighted mean of the pollution raster cells overlapping each reference grid cell. Figure A.1 shows the spatial distribution of PM2.5 and PM10 across Germany at the start and end of the sample period. Average concentrations of both pollutants decline substantially over the period, but considerable regional heterogeneity in exposure persists. While the two measures differ in absolute levels by construction, as PM2.5 mass is a subset of PM10 mass, their relative spatial distributions are closely aligned.

WEATHER DATA

To account for time-varying meteorological conditions that affect ambient particulate concentrations independently of emissions, I incorporate high-resolution reanalysis data from the ERA5-Land dataset (Muñoz-Sabater et al., 2021). ERA5-Land provides a consistent representation of land-surface variables at a spatial resolution of approximately 9 km $\times$ 9 km ($0.1^\circ \times 0.1^\circ$).[6]

I retrieve monthly data for 2m air temperature, total precipitation, and the eastward (u10) and northward (v10) wind vector components for the period 2010–2021. I aggregate these observations to the annual level by computing the mean temperature, average daily precipitation, and the magnitude of the annual mean wind vector at the ERA5 cell level. The latter measures the strength and persistence of the prevailing wind and thus captures the ventilation conditions relevant for pollutant dispersion. The weather variables are then merged onto the RWI 1 km $\times$ 1 km reference grid as the area-weighted mean of overlapping ERA5-Land cells, following the same procedure used for the pollution rasters.

[6] Retrieved via an API call from the Copernicus Climate Data Store. Last accessed 29 December 2025.

INDUSTRIAL FACILITY DATA

Finally, I retrieve data on polluting industrial facilities in Germany from the EU Industrial Reporting Database (IRD).[7] The IRD consolidates two previously existing databases: the European Pollutant Release and Transfer Register (E-PRTR) and the reporting required under the Industrial Emissions Directive (IED).[8] Both of these EU legal instruments regulate the reporting of industrial activities and the associated emissions and are applied at the level of industrial facilities.[9] The IRD merges the reporting outputs of the two instruments under a common infrastructure without altering the underlying legislation or reporting requirements. In Germany, it covers 13,318 facilities (out of 99,500 across the EU), comprising large industrial operations such as power generation, chemical industry, waste incineration and large-scale livestock facilities.

For each facility, the database reports the location and operational status, together with the parent company, the main industrial activity, and the type, amount, and medium (air, water, or soil) of reported releases where available. A key advantage of the IRD over its predecessor databases concerns facility status. Under E-PRTR, reporting was triggered by either the size of a facility's installations (e.g., the incineration capacity of a waste incinerator) or the amount of a specific pollutant released in a given year (e.g., NO_x). Facilities that qualified only via the latter dropped out of the data in years in which their emissions fell below the corresponding threshold, making temporary fluctuations around the reporting threshold indistinguishable from permanent shutdowns. The IRD overcomes this by retaining closed facilities in the database and reporting their operational status as *functional*, *disused*, *decommissioned*, or *notRegulated*. This status variable is recorded for non-operational sites only from 2016 onward, which restricts the start of the closure observation window in the empirical analysis to 2017 (as for a closure to be observed, operational status needs to transition between years).

I define a facility as closing in the first year in which its reported status changes from *functional* to *disused* or *decommissioned*. This year constitutes the treatment date τ_n for all grid cells assigned to the facility. No facility in the estimation sample reverts to *functional* status after this transition. Because the recorded status change may lag the physical cessation of operations,

[7] I use the 2023 release of the data (version 8) available at https://www.eea.europa.eu/data-and-maps/data/industrial-reporting-under-the-industrial-7/eu-registry-e-prtr-lcp.

[8] Legislation: https://eur-lex.europa.eu/eli/dir/2010/75/oj (IED) and https://eur-lex.europa.eu/legal-content/EN/TXT/?uri=celex:32006R0166 (E-PRTR).

[9] The specific reporting requirements are documented in Annex I of the corresponding legal texts cited above.

treatment timing is measured with potential delay.

I project facility coordinates onto the RWI reference grid and assign a facility to a grid cell whenever the cell's area overlaps with a buffer of radius r around the facility's reported point coordinates. Combining these assignments with the reference grid yields a panel of approximately 1.8 million grid cell-by-year observations covering all populated areas of Germany throughout the sample period. To reduce the strength of the assumptions required for identification, I construct an estimation sample restricted to grid cells in the immediate vicinity of closing facilities (see Section IV for a detailed discussion). Specifically, I identify 345 distinct plants that close according to this definition during the observation window, and limit the estimation sample to grid cells within a five-kilometer radius of these sites in the baseline specification. Given the empirical strategy (see Section IV), all units are treated by 2021, so that observations from calendar year 2021 do not contribute any variation that can be leveraged for treatment effect estimation. Therefore, observations from 2021 are excluded from the estimation sample. This yields approximately 16,500 distinct grid cells and a final panel of 180,000 observations, which I define as the main estimation sample. Alternative buffer sizes of 10 km and 2 km are considered in Appendices B and C. This selection criterion ensures that all observations in the analysis are proximate to at least one large industrial facility that ceases operations during the study period. Table A.1 reports summary statistics for the full panel and the restricted estimation sample, and Figure A.5 shows the spatial distribution of treated grid cells across Germany.

III DESCRIPTIVE EVIDENCE: EXPOSURE INEQUALITY IN GERMANY

Shutdowns of large industrial sites are expected to affect local environmental amenities such as air quality. Before estimating the causal impacts of IRD closures, this section quantifies the baseline distribution of pollution exposure across neighborhoods in Germany.

While US-focused research documents unequal pollution exposure at multiple scales, many European studies linking socioeconomic conditions to environmental hazards face one of two limitations. First, analyses conducted at the level of relatively large administrative units tend to mask substantial within-unit variation in the socioeconomic variable of interest (e.g., household income) and are vulnerable to ecological fallacy concerns (Banzhaf et al., 2019). Second, more disaggregated studies often rely on a single year of data (see, e.g., Rüttenauer, 2018;

Neier, 2021), which precludes comparisons over time.[10] Appendix Figure A.2 illustrates the aggregation problem by plotting the distribution of PM2.5 exposure across pollution and income percentiles within the municipality of Berlin in 2021. The figure shows considerable within-city variation — variation that would be concealed if analyses were conducted at the municipal level.[11]

It is thus natural to ask what the PM2.5 exposure gradient across the income distribution looks like when measured at a granular level. I investigate this by regressing the mean annual PM2.5 concentration on indicator variables for the national-level income decile that a given grid cell belongs to in a model of the following form

$$\mathrm{PM}_{2.5,nt} = \sum_{k=2}^{10} \psi_k \cdot \mathbb{1}[D_{nt} = k] + C_{nt}\delta + \omega_t + \epsilon_{nt} \tag{1}$$

where $\mathrm{PM}_{2.5,nt}$ denotes the mean annual concentration of PM2.5 in grid cell n in year t, D_{nt} indicates which (population-weighted) national income decile grid cell n belongs to in year t, and C_{nt} is a vector of meteorological controls including mean annual temperature, average daily precipitation, and the magnitude of the annual mean wind vector. Finally, ω_t represents year fixed effects, which absorb the general trend towards cleaner air observed across the whole of Germany.

The distributional analysis in this and the following sections is conducted for fine particulate matter, measured by the satellite-derived product of van Donkelaar et al. (2021). This choice reflects the fact that PM2.5 is the size fraction most strongly linked to adverse health outcomes and the standard exposure measure in the environmental justice literature to which these results speak (Colmer et al., 2020; Jbaily et al., 2022; Currie et al., 2023). Moreover, the satellite product is reported at a comparable resolution to the socioeconomic data, so that the estimated gradient exploits precisely the granular variation that Appendix Figure A.2 shows to be concealed at coarser levels of aggregation.

Figure 1 shows the results from estimating Equation (1) on the full sample of 1,800,000 grid cell-year observations covering all populated areas of Germany over the entire period 2010–2021. The point estimates display the exposure gap relative to grid cells in the bottom in-

[10] Examples of studies at higher spatial aggregation include European Environment Agency (2018); Germani et al. (2014); Lavaine (2015); Richardson et al. (2013); for a European meta-analysis, see Fairburn et al. (2019).

[11] Hsiang et al. (2019) also show that the cross-sectional relationship between household income and air pollution exposure in the United States is highly sensitive to the level of administrative aggregation.

Figure 1: Cross-Sectional Ambient PM2.5 Exposure Across the Income Distribution

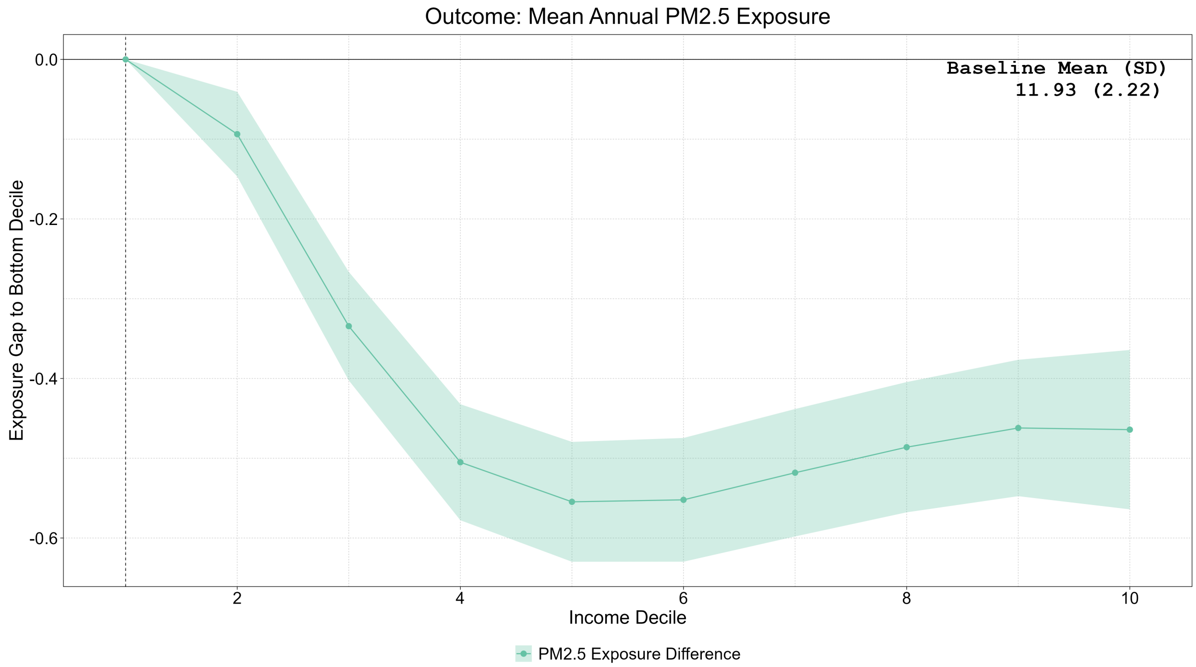

Note: The graph displays point estimates and 95% confidence intervals for ψ_k from Equation (1) estimated on the full sample of 1,800,000 grid cell - year observations covering the full sample period. The outcome is mean ambient PM2.5 as measured by van Donkelaar et al. (2021). Estimates represent exposure differentials relative to the bottom decile. The model includes mean annual temperature, average daily precipitation, and the magnitude of the mean wind vector as controls. Standard errors are clustered by municipality. Regression outputs are reported in Table A.3.

come decile across the income distribution. The statistically significant gradient indicates that grid cells in the bottom income decile are exposed to higher PM2.5 concentrations than every other decile, with the gap widening monotonically up to the middle of the distribution, where it reaches 0.55 $\mu g/m^3$, or 0.25 standard deviations of the full-sample PM2.5 distribution. Above the median, the gap narrows again, producing a U-shaped profile in which the most affluent deciles are more exposed than the middle of the distribution though still considerably less than the bottom decile. This pattern is consistent with existing cross-sectional evidence on exposure disparities and may be explained by higher pollution concentrations in comparatively more affluent urban agglomerations (Hsiang et al., 2019; Champalaune, 2026). Bos et al. (2025) find a similar pattern for PM2.5 exposure across grid cells in a study of the distributional effects of low emission zones in Germany.

Notably, this exposure gradient persists within the estimation sample used in the causal analysis below. Appendix Figure A.3 reports estimates of Equation (1) restricted to grid cells within 5km of closing IRD plants over the pre-treatment period 2010–2016. Even within these more industrial neighborhoods, the largest gap, which occurs between the bottom decile and the 7th decile, amounts to approximately 0.53 $\mu g/m^3$, corresponding to an additional exposure burden for residents of low-income grid cells of 0.28 standard deviations of the pre-treatment PM2.5 distribution. Appendix Figure A.4 reports the corresponding gradient for PM10 based on the monitor-derived data of Umweltbundesamt (2023). Although the two outcomes differ in both the size fraction measured and the underlying measurement technology, the qualitatively similar pattern indicates that the exposure gradient is not an artifact of the satellite product.

In summary, the results show a robust pattern of environmental inequality in Germany. Economic deprivation and exposure to ambient air pollution tend to coincide at the neighborhood level, both nationally and within the industrial neighborhoods studied below. Pollution burdens fall disproportionately on low-income residents, so that any air quality gains and economic losses from closures will be distributed across this neighborhood gradient. How closures in fact affect both the distribution of pollution exposure and local economic conditions is the causal question to which the remainder of the paper turns.

IV EMPIRICAL STRATEGY

The primary objective of this paper is to estimate the causal effect of large industrial facility shutdowns on local environmental and socioeconomic outcomes. To this end, I exploit the staggered timing of facility closures across different locations within an event study framework. The model of interest is

$$Y_{nt} = \sum_{s \neq -1} \theta_s \cdot \mathbb{1}[t - \tau_n = s] + C_{nt}\beta + \mu_n + \omega_t + \epsilon_{nt} \tag{2}$$

where Y_{nt} is the outcome of interest in grid cell n and year t. The term $\mathbb{1}[t - \tau_n = s]$ is an indicator variable that equals one if year t lies s years from τ_n, the year of the first closure affecting cell n as defined in Section II. The indicator for $s = -1$ is omitted, so that all effects are expressed relative to the year immediately preceding the shutdown. μ_n and ω_t represent grid cell and year fixed effects, respectively. In the air quality specifications, C_{nt} contains mean temperature, average daily precipitation, and the magnitude of the annual mean wind vector. The socioeconomic and housing specifications include no time-varying controls. The coefficients of interest, θ_s, represent the effect of the closure s years from the event.

I estimate Equation (2) using the two-stage procedure proposed by Gardner et al. (2024). In a first stage, the fixed effects and the coefficients on C_{nt} are estimated using not-yet-treated observations only; in a second stage, the event-time coefficients θ_s are obtained from a regression of the residualized outcome on the treatment indicators. Estimating the fixed effects free of contamination from post-treatment observations avoids the bias that arises in the corresponding one-step regression under staggered adoption and heterogeneous treatment effects (de Chaisemartin and D'Haultfœuille, 2020; Goodman-Bacon, 2021).[12]

Note that coding τ_n as the year of the *first* closure implies that grid cells located in the intersection of multiple treatment buffers may experience further closures after their initial treatment date. I therefore examine the sensitivity of the estimates to restricting the sample to grid cells that experience a single closure throughout the sample period. I also estimate a variant of Equation (2) with year-by-sector fixed effects to absorb any sector-level shocks that may affect local outcomes.[13]

Retaining only grid cells located in the vicinity of closing plants entails that all grid cells receive treatment by the end of the sample period. In other words, there are no *never treated* grid cells in the sample. Therefore, the control units used to estimate θ_s are those grid cells for which $\tau_n > t$ (i.e., *not yet treated* grid cells). This design mitigates a first-order selection concern by avoiding comparisons between grid cells that experience an IRD closure and grid cells that do not experience a shutdown (or never hosted an industrial plant in the first place). The identifying variation that allows for the estimation of Equation (2) thus comes from differences in *shutdown timing* across facilities rather than variation in the mere location of shutdowns across space. Standard errors are clustered by municipality throughout. Municipalities are the administrative unit with substantial discretion over housing and land use policy in Germany, so that grid cells within a given municipality likely share a correlated component of the residual variation in local outcomes.

[12] In this setting, the procedure yields point estimates equivalent to the imputation estimator of Borusyak et al. (2024). I use the two-stage implementation for its computational efficiency.

[13] Because activity codes are observed only for former E-PRTR facilities (see Section II), the inclusion of sector-by-year fixed effects reduces the sample size. I therefore treat this specification as a robustness check rather than the main specification.

The key identifying assumption for θ_s to represent the causal effect of IRD shutdowns on local outcomes is that the precise relative timing of an IRD shutdown is orthogonal to trends in local outcomes. Note that identification does not require closure locations to be orthogonal to local characteristics. By restricting the analysis to grid cells within the vicinity of plants that close during the observation window, I compare places that were all selected for industrial siting at some point, and identifying variation comes from differences in closure timing rather than differences in exposure to industrial activity. Historical selection of sites into industrial areas is therefore absorbed by construction.

Three concerns about the exogeneity of timing remain. The first is that closures may be preceded by neighborhood-specific decline or gentrification that simultaneously affects the propensity of local plants to be shut down and independently moves the outcomes. This concern is a classical potential parallel-trends violation. If treated cells were already on a different trajectory than not-yet-treated cells in the years before closure, the post-closure estimates would conflate the causal effect of the shutdown with the continuation of a pre-existing trend. The institutional context renders this unlikely as the plants in the sample are large industrial sites such as heavy manufacturing, power generation, or industrial-scale livestock operations, whose decommissioning is determined at the corporate, federal, or supranational level rather than in response to neighborhood conditions (see Table A.2 for a sectoral breakdown). To support this argument, Figure A.6 plots the evolution of all outcome variables over 2010–2016, the years preceding the closure observation window, separately for each treatment adoption cohort. If treatment timing were correlated with local trends, cohorts should diverge over this common pre-period. Figure A.6 shows no systematic differences in raw outcome trends across adoption cohorts. The pre-treatment event study coefficients reported in Section V provide the corresponding formal test and show no evidence of systematic differential trends in the years leading up to closure.

A related concern is anticipation. The closure of a large industrial site is typically announced before operations cease, and forward-looking outcomes such as housing prices in particular may respond at announcement rather than at the recorded status change. Such anticipation would appear as pre-treatment effects in the event studies. Reassuringly, the absence of systematic pre-treatment movement in prices and rents indicates that capitalization ahead of the recorded closure is limited in practice. To the extent that some response nonetheless occurs before τ_n, it is absorbed into the pre-period and the reference year, compressing the measured contrast between pre- and post-closure outcomes. Together with the possibility that the recorded status change lags the physical cessation of operations (Section II), this implies that the post-closure estimates are, if anything, attenuated.

The second concern is that a sector-wide shock may simultaneously induce plant closures and affect the local economy through channels other than the focal plant's shutdown. Two cases must be distinguished. If the focal closure itself causes surrounding suppliers or downstream firms to contract, this contraction is part of the local effect of the shutdown and represents the estimand of interest rather than a confound. The threat to identification arises only when a common sectoral shock drives both the closure and an independent contraction in the local economy. To address this concern, I augment the baseline specification with sector-by-year fixed effects, which absorb the aggregate component of any shock common to plants in the same industry in a given year. Robustness of the results to this inclusion indicates that the estimates are not driven by closures clustering in nationally declining sectors.

The third concern is interference across treatment units. Control cells are not yet treated with respect to the facility defining their own treatment date, but some lie within reach of other facilities that have already closed, and the distance-ring estimates in Appendix E indicate that air quality effects do not decay sharply within 10km. Such interference is, however, a testable concern in this design. Because closures are observed only from 2017 onward while outcomes are observed from 2010, any contaminating closure necessarily falls within the observed pre-treatment window of the affected cell. Quantitatively meaningful contamination from a nearby closure would therefore surface as a jump in the pre-treatment event study coefficients.

For estimation, I bin all pre-treatment years that precede the closure by five years or more into a single category. The estimated dynamic effects cover the closure year and the three subsequent years. Because all grid cells in the sample are treated by 2021, the final sample year contains no not-yet-treated observations. Post-treatment effects for the 2021 cohort are therefore not identified, and this cohort enters the estimation only through its pre-2021 observations, which serve as controls for earlier cohorts. All baseline results are generated using a buffer size of 5 km. Appendices B and C provide robustness checks using buffer sizes of 10 km and 2 km, respectively.

V RESULTS

AIR QUALITY IMPACTS

Section III documents a significant gradient in PM2.5 exposure across the neighborhood-level income distribution, which persists even within the sample of grid cells located in the immediate vicinity of IRD plants. While road traffic is one of the main sources of fine particulate matter in Germany, industrial sources are significant contributors to the overall pollution load. The European Environment Agency (EEA) estimates that air pollution from large industrial facilities alone caused damages of up to €350 billion in 2021 in Europe (European Environment Agency, 2024). This section therefore examines whether IRD shutdowns detectably improve air quality in surrounding neighborhoods.

I estimate Equation (2) with mean annual PM2.5 and PM10 exposure at the grid cell level as outcomes of interest. Table 1 reports the combined average treatment effect on the treated (ATT) across all post-treatment periods for both pollutants. Columns (1) and (5), which show the unconditional treatment effects, suggest significant reductions in average annual PM2.5 exposure of 0.08 $\mu g/m^3$ and in PM10 exposure of 0.23 $\mu g/m^3$ following IRD shutdowns. These effects are robust to the inclusion of weather controls (Columns (2) and (6)), to restricting the sample to grid cells that experience a single closure (Columns (3) and (7)), and to the inclusion of year-by-sector fixed effects (Columns (4) and (8)), although the PM10 point estimates fluctuate somewhat more across specifications. Because PM2.5 mass is a subset of PM10 mass by construction, the two pollutants differ mechanically in baseline levels and dispersion. To make effect sizes comparable, I thus normalize by the respective pre-treatment standard deviations. In the single-closure specification (Columns (3) and (7)), the PM10 response of -0.10 SD is roughly twice as large as the PM2.5 response of -0.046 SD. This ordering is consistent with the size-fraction argument of Section II. Given that the empirical design measures particulate matter concentration within a fixed radius of the closing plant, it recovers the avoided primary emissions but not the avoided secondary formation, which materializes downwind and contributes predominantly to the fine fraction. The PM2.5 estimate is therefore attenuated relative to the PM10 estimate by construction. Since the two measures differ in both the pollutant and the underlying measurement technology, however, this comparison should be read as suggestive. Figure A.7 displays the corresponding event study estimates for the specification with weather controls, estimated on grid cells within a single treatment buffer. The ATTs printed in Figure A.7 accordingly correspond to Columns (3) and (7) of Table 1. The coefficients in the years immediately preceding closure are tightly centered around zero for both pollutants. The PM10 series displays some fluctuation but exhibits no systematic pre-trend that could account for the post-closure decline. Following the shutdown, both series drop sharply. The PM2.5 concentration partially rebounds towards the end of the event window, while the PM10 reduction persists throughout. Figure E.1 shows that these averages are not driven by cells closest to the plant. Ring-specific ATTs are approximately uniform out to 10 km for both pollutants, which motivates the uniform treatment buffer design in the main analysis.

These results indicate that IRD shutdowns induce moderate but statistically significant air quality gains in the immediate vicinity of closed plants. As stated above, these estimates primarily capture the effect of avoided primary particulate emissions at the source and exclude reductions in secondary particulate matter. The estimates should therefore be interpreted as pure local effects and likely understate the full air quality benefits of IRD closures throughout Germany and neighboring countries (Holland et al., 2020; Hernandez-Cortes and Meng, 2023; Morehouse and Rubin, 2026).

Table 1: Effect of IRD Closure on Air Quality

Dependent Variables:	PM2.5 (van Donkelaar)				PM10 (UBA)			
Model:	(1)	(2)	(3)	(4)	(5)	(6)	(7)	(8)
Closure	-0.0797***	-0.0704***	-0.0847***	-0.0780***	-0.2315***	-0.2245***	-0.2874***	-0.1862**
	(0.0280)	(0.0249)	(0.0281)	(0.0287)	(0.0795)	(0.0773)	(0.0766)	(0.0916)
Single Treatment			✓				✓	
Weather Controls		✓	✓	✓		✓	✓	✓
Year	✓	✓	✓		✓	✓	✓	
Year × Sector				✓				✓
Grid Cell	✓	✓	✓	✓	✓	✓	✓	✓
Observations	179,933	179,933	135,345	153,457	179,817	179,817	135,271	153,383
R^2	0.00391	0.00339	0.00439	0.00473	0.00579	0.00560	0.00885	0.00408
Adjusted R^2	0.00391	0.00339	0.00439	0.00473	0.00579	0.00560	0.00885	0.00408

*Signif. Codes: ***: 0.01, **: 0.05, *: 0.1*
Clustered standard errors (Municipality) in parentheses.

Note: The table shows ATT estimates for the effect of IRD closures on mean annual particulate matter concentration across all post-treatment periods for grid cells located within 5km of a closing IRD plant. Columns (1) - (4) report results for PM2.5 provided by van Donkelaar et al. (2021) and columns (5) - (8) report results for PM10 from Umweltbundesamt (2023). Columns (3) and (7) exclude grid cells located within 5km of multiple closing plants. Reduced sample size in columns (4) and (8) is due to incomplete sector assignments at the facility level. Standard errors are clustered by municipality.

The aggregate ATTs in Table 1 moreover average over a heterogeneous set of closing facilities. The plants in the sample span activities as diverse as fuel combustion installations, lime works, foundries, landfills, and slaughterhouses (see Table A.2), which differ widely in their primary particulate footprint. The estimated reductions plausibly derive disproportionately from dust-intensive operations in the mineral, energy, or waste sectors, whereas facilities with modest primary PM releases should leave concentrations in the immediate vicinity essentially unchanged. The estimates above are therefore best read as a diluted average across facility types rather than as the local air quality gain from removing a representative heavy emitter.[14] For the purposes of this paper, however, the relevant conclusion is that IRD shutdowns detectably improve local air quality at the mean, confirming that the closing facilities constitute genuine environmental disamenities for their host neighborhoods on average. It is further important to note that particulate matter is only one dimension of this disamenity. IRD facilities report releases to air, water, and soil, and their operation is typically accompanied by burdens such as odor, noise, and heavy traffic that closures also remove. The pollution response documented here should thus be understood as one measurable component of a broader improvement in local environmental conditions following a shutdown.

THE EFFECT OF INDUSTRIAL SHUTDOWNS ON THE PM2.5 EXPOSURE GAP

The estimates in Table 1 capture the average effect of IRD shutdowns on air quality in surrounding grid cells. Figure A.3, however, reveals substantial heterogeneity in baseline pollution exposure across the income distribution. To examine whether industrial closures affect this exposure gap, I augment Equation (2) by interacting treatment with an indicator for the baseline income decile of each grid cell, defined by the cell's position in the estimation sample's income distribution in the year preceding its closure ($s = -1$).[15] Figure 2 presents the resulting ATTs across all post-treatment periods by income decile, both for the full estimation sample and for the subsample of grid cells that experience a single closure.

The estimates indicate that the air quality gains from industrial closures are markedly progressive. Grid cells in the bottom half of the income distribution experience substantially larger reductions in PM2.5 than more affluent areas. Gains at the bottom of the distribution are two to three times as large as the aggregate ATT, while effects in the top deciles are sta-

[14] In principle, the IRD reports facility-level releases which would allow me to condition on pre-closure particulate release. However, the reported releases are incomplete in the data which precludes such an exercise.

[15] I use the PM2.5 measure of van Donkelaar et al. (2021) for the reasons set out in Section III.

tistically indistinguishable from zero. This pattern is consistent with the baseline gradient documented in Figure A.3, as lower-income grid cells are located in more polluted places on average and therefore stand to gain more when local pollution sources are removed. Given that the distance-ring estimates in Appendix E show no decay of the air quality effect within the buffer, this result is not a mere artifact of differences in proximity to the pollution source. IRD shutdowns thus contribute to narrowing the local PM2.5 exposure gap between the most deprived and the most affluent neighborhoods. It is important to note, however, that these estimates capture the within-buffer redistribution of air quality gains and do not speak to the national-level exposure gap shown in Figure 1, an evaluation of which would require modeling the dispersion of avoided emissions across the entire country.[16]

Figure 2: Treatment Effect Heterogeneity for PM2.5 by Income Decile

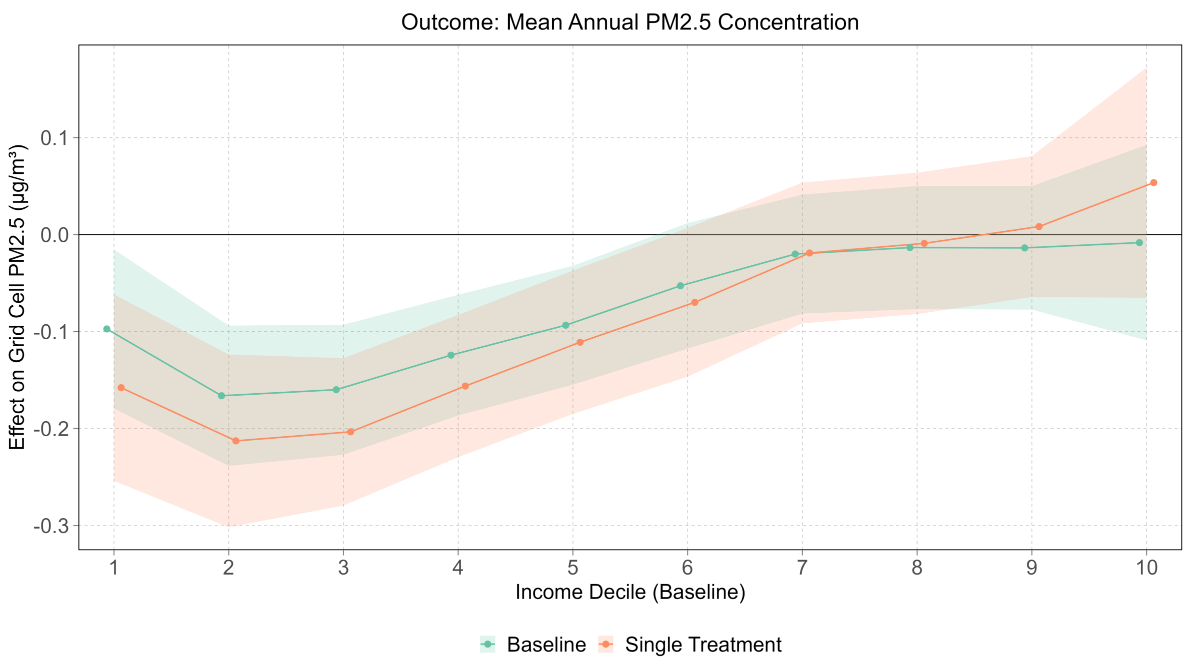

Note: The figure shows the average treatment effect and 95% confidence interval for the effect of an IRD shutdown on PM2.5 concentration in surrounding grid cells averaged across all post-treatment periods by baseline income decile of the treated grid cells. Income deciles are defined within the estimation sample in the year preceding each cell's closure ($s = -1$). Estimates correspond to results obtained using the model from Equation (2) with treatment interacted with baseline income decile. Standard errors are clustered by municipality. Single Treatment refers to estimates obtained excluding grid cells that experience more than one closure during the sample period.

[16] Figures B.2 and C.2 show that this conclusion is robust to the size of the treatment buffer.

The air quality gains documented in Figure 2 represent one channel through which IRD shutdowns can affect local welfare. IRD plants, however, can also represent an important share of local labor demand and play a central role in local economies. The net effect of a shutdown is therefore a priori ambiguous. If the accompanying labor demand shock is small, the amenity gain should capitalize into higher housing prices. If the labor market channel dominates, prices could fall despite improved environmental quality.

Existing evidence is consistent with both cases. US-based studies generally find that removing local pollution sources raises neighborhood desirability, whether through hazardous waste cleanups (Gamper-Rabindran and Timmins, 2011), changes in toxic plant presence (Currie et al., 2015), or coal plant retirements (Fraenkel et al., 2024). A separate literature, however, documents substantial earnings losses among workers displaced from carbon-intensive industries (Barreto et al., 2023; Colmer et al., 2024; Haywood et al., 2024; Rud et al., 2024) and broader regional decline in coal-dependent communities (Krause, 2026b). Motivated by these opposing forces, I assess the local economic consequences of IRD shutdowns by examining effects on housing prices, income, and unemployment.

To assess how IRD shutdowns affect housing prices, I estimate Equation (2) separately with average log house prices and apartment rents per square meter as outcomes at the grid cell level. Figure 3 plots the estimates for θ_s, i.e., the dynamic effect of IRD shutdowns on surrounding house prices and rents. Both house prices and rents decline following the shutdown, with effects growing in magnitude over subsequent years. By the end of the event window, local house prices are reduced by approximately 3.1% relative to the year before the closure. The average decline across all post-treatment periods amounts to a statistically significant 1.6% in the baseline specification (2.7% when including sector-by-year fixed effects; see Table A.4). The estimates for rents are noisier but point in the same direction. While the average effect across post-treatment periods is not statistically distinguishable from zero, apartment rents exhibit an imprecisely estimated depression of 2% by the end of the event window. The weaker response of rents relative to prices is plausibly consistent with house prices capitalizing expected future deterioration in local conditions in addition to their current state. Appendix F provides a property-level robustness check of the housing price response to account for compositional changes in the housing stock listed for sale/rent.

Although these estimates should not be interpreted directly as willingness to pay for facility

Figure 3: Effect of IRD Closure on House Prices and Apartment Rents

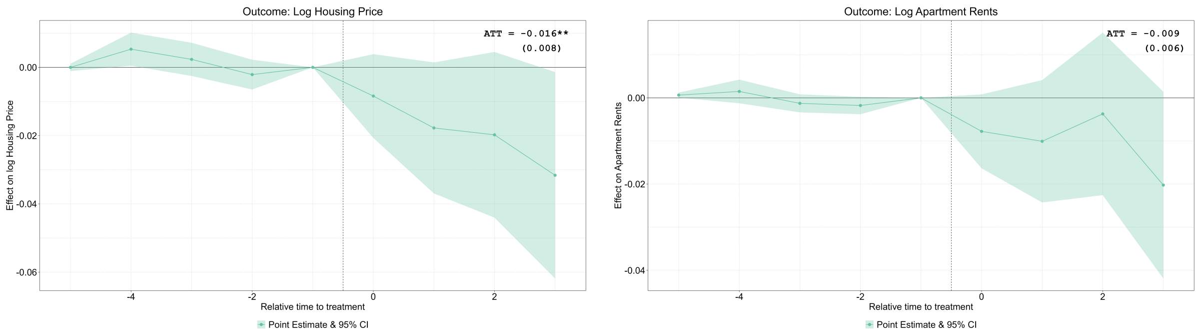

(a) House Prices (in logs)

(b) Apartment Rents (in logs)

Note: The figure shows point estimates and 95% confidence intervals for θ_s from Equation (2). The outcome variables are the natural logarithm of average house prices per square meter (Panel (a)) and average apartment rents per square meter (Panel (b)) at the grid cell level. The sample consists of all grid cells within a 5 km radius around plants that close down during the sample period. Standard errors are clustered by municipality. The ATT estimates in the top right corner of each panel represent the joint effect across all post-treatment periods.

presence (Kuminoff and Pope, 2014; Banzhaf, 2021), they indicate that facility shutdowns have a clear negative effect on the residential desirability of affected neighborhoods. This finding is in line with existing evidence for Germany, where Bauer et al. (2017) and Bruns and Thomsen (2025) document declines in local property values following the shutdown of nuclear and coal power plants, respectively. It stands in contrast, however, to the positive housing price effects that Fraenkel et al. (2024) document for US coal unit retirements — an appreciation the authors explicitly link to the absence of accompanying labor market disruptions in their setting. Jowers et al. (2025) find that housing prices fall in response to the *opposite* event, the opening of industrial livestock operations. That both the arrival and the removal of an industrial facility can depress local property values is difficult to rationalize in a pure amenity framework, but is plausible once facilities are understood to bundle an environmental disamenity with local labor demand (Bartik et al., 2019). Whether the labor margin is operative for IRD closures is directly testable, and I turn next to their local labor market effects.

Figure 4 traces how disposable household income per adult and unemployment respond to IRD shutdowns. Panel (a) documents an immediate and economically meaningful reduction in local income following an IRD closure. The magnitude of these income losses increases over time to reach an income reduction of 2.2% by the end of the event window. While these income losses are localized, they are not negligible in aggregate. With baseline income per adult of

€ 26,700 (constant 2016 EUR), an average population of roughly 1,000 adults per grid cell, and approximately 16,500 grid cells within 5km of closing plants, the affected population totals around 16.5 million adults. The aggregate ATT across all post-treatment periods suggests a mean annual income loss of 0.8% (see Table A.5), which translates into an aggregate *annual* income loss of € 3.6 billion (95% CI: [€ -5.9 billion; € -1.3 billion]) once all closures are realized. These figures capture localized partial-equilibrium losses in neighborhoods directly affected by IRD closures and do not net out income gains accruing elsewhere or general equilibrium reallocation across sectors and space. They further assume that the aggregate ATT applies uniformly across all post-treatment periods once a closure is realized. Given these caveats, it is clear that these aggregate losses should only be read as illustrative orders of magnitude.

Panel (b) shows that part of the income loss reflects rising unemployment in the vicinity of closing IRD sites. The unemployment rate is essentially unchanged in the first two years following the shutdown, consistent with the German institutional context, in which large layoffs typically involve extended notice periods and severance schemes that can postpone the transition into registered unemployment. By the end of the event window, however, the unemployment rate is 0.3 percentage points higher in affected grid cells. This increase is unlikely to account for the full magnitude of the income losses in Panel (a). The reduction in neighborhood income therefore likely reflects a combination of mechanisms. Alongside transitions into unemployment, affected workers face earnings losses from moving to lower-paying jobs or exiting the labor force through early retirement (Schmieder et al., 2023). This interpretation aligns with recent worker-level evidence on the persistent earnings scars associated with displacement from carbon-intensive industries (Barreto et al., 2023; Colmer et al., 2024; Haywood et al., 2024; Rud et al., 2024).

An alternative explanation is that the income decline reflects changes in residential composition rather than losses to incumbent residents. For instance, if former employees of the closing plant have above-average incomes within their neighborhoods and migrate away after the shutdown, this out-migration alone could account for the drop in average neighborhood income. Figure A.8 shows that total population remains approximately constant in affected neighborhoods following a closure. While this only establishes that *net* migration is approximately zero and does not rule out compositional changes, the absence of any population response suggests that the observed income and employment losses are driven primarily by impacts on incumbent residents.

Figure 4: Effect of IRD Closure on Disposable Household Income and Unemployment

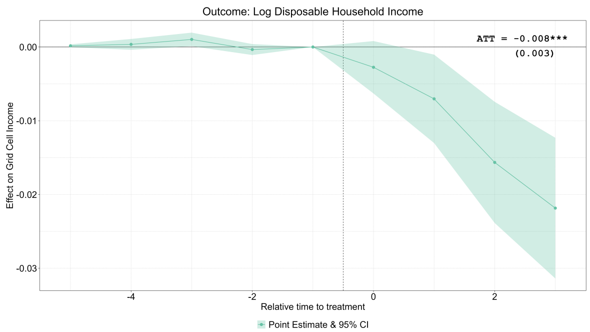

(a) Disposable Household Income (in logs)

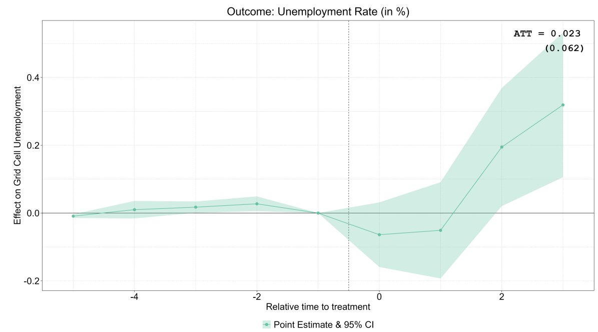

(b) Unemployment Rate

Note: The figure shows point estimates and 95% confidence intervals for θ_s from Equation (2). The outcome variables are the natural logarithm of average disposable household income per adult (Panel (a)) and the unemployment rate (Panel (b)) at the grid cell level. The sample consists of all grid cells within a 5 km radius around plants that close down during the sample period. Standard errors are clustered by municipality. The ATT estimates in the top right corner of each panel represent the joint effect across all post-treatment periods.

Taken together, the results in Figure 4 indicate that IRD shutdowns generate significant adverse shocks to local labor markets.[17] This establishes that the condition under which previous studies find a green dividend fails in the present setting. IRD closures deliver environmental amenity gains and labor market losses simultaneously, and the housing price decline documented above indicates that the latter dominate in the housing market. The pattern parallels Bauer et al. (2017), who find in an analogous trade-off that the local employment effects of post-Fukushima nuclear shutdowns in Germany dominate the amenity effects of reduced perceived nuclear risk. Whether the non-market dimensions of local desirability deteriorate on net, however, cannot be read off prices alone. I therefore revisit this trade-off below using a location choice framework that recovers the movement in non-market amenities consistent with the observed changes in income, housing prices, and population.

THE CLOSURE PENALTY IN INDUSTRIALLY DEPENDENT REGIONS

Existing evidence shows that the local economic and demographic context shapes how regions absorb adverse shocks to their industrial base (Gagliardi et al., 2023; Krause, 2026b). Figure 4 displays the aggregate labor market effects of IRD closures, but these aggregates may

[17] The 5km resolution of this finding is consistent with vom Berge and Schmillen (2023), who show that the labor market effects of mass layoff events in Germany are highly localized.

mask substantial heterogeneity if certain heavily affected areas drive the average response. To examine whether some regions incur an additional closure penalty, I estimate the following specification

$$Y_{nt} = \sum_{s \neq -1} (\theta_s + \gamma_s \text{IndEmpl}_n) \cdot \mathbb{1}[t - \tau_n = s] + \mu_n + \omega_t + \epsilon_{nt} \tag{3}$$

where Y_{nt} is log mean disposable household income per adult or the unemployment rate in grid cell n, and IndEmpl_n is a binary indicator equal to one if grid cell n lies in a district where at least 25% of the working-age population is in industrial employment in the year preceding the cell's closure ($s = -1$). This applies to 16.9% of grid cells in the sample. Because the industrial employment share is observed at the district level only, the indicator does not vary within treatment buffers and the interaction coefficients γ_s thus compare neighborhoods around closures in industrially dependent districts to neighborhoods around closures elsewhere, rather than differently exposed neighborhoods around the same plant. Figure 5 reports the event study estimates and Table A.5 in the Appendix shows aggregate ATTs across specifications and robustness checks.

The results in Figure 5 show that the aggregate labor market costs of industrial shutdowns are disproportionately concentrated in regions with high baseline dependence on industrial employment. Panel (a) shows that the baseline effect (θ_s) on disposable household income is negative but moderate, reaching a reduction of approximately 1.7% by the end of the event window. Closures in industrially dependent districts induce a substantially steeper decline. The interaction coefficients (γ_s) indicate an additional closure penalty that grows over time, reaching a further 2.6% by the end of the event window. The total income loss in heavily industrialized neighborhoods thus reaches 4.3%, more than doubling the effect observed in less industrial regions.

Panel (b) documents the corresponding pattern for unemployment. The results show that the delayed response in Figure 4 reflects the comparatively modest and sluggish response in areas with low industrial reliance, whereas high-industrial areas experience an immediate and sharp increase, with the interaction effect peaking two years after the shutdown at roughly 0.8 percentage points. The unemployment interaction notably exhibits statistically significant pre-treatment coefficients. Appendix D shows that these are attributable to differential trends in the unemployment rate across districts with and without high industrial employment at baseline. Reassuringly, both the baseline and interaction effects are robust to absorbing dif-

Figure 5: Effect of IRD Closure on Disposable Household Income and Unemployment – Heterogeneity by Baseline Industrial Employment Share

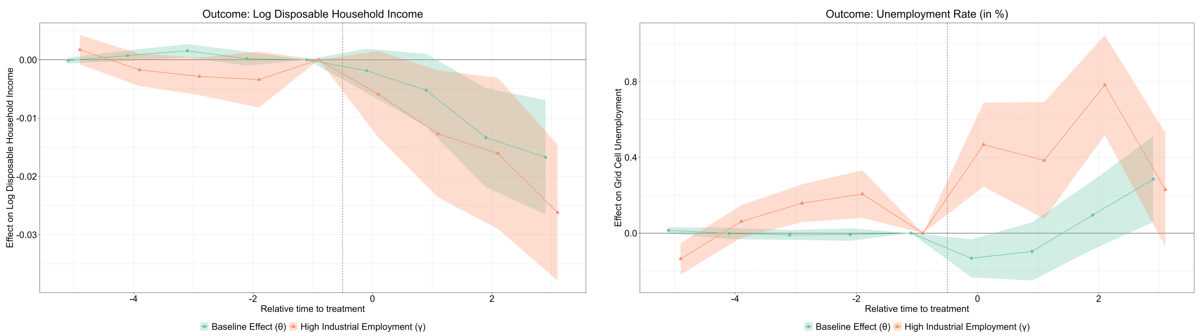

(a) Disposable Household Income (in logs)

(b) Unemployment Rate

Note: The figure shows point estimates and 95% confidence intervals for θ_s and γ_s from Equation (3). The outcome variables are the natural logarithm of average disposable household income per adult (Panel (a)) and the unemployment rate (Panel (b)) at the grid cell level. The sample consists of all grid cells within a 5 km radius around plants that close down during the sample period. Standard errors are clustered by municipality.

ferential year effects for the two groups. The unemployment closure penalty for areas with comparatively strong industrial dependence is thus not an artifact of these differential trends but indeed a causal effect of IRD closures.

While the grid-cell data do not include information on education or skills, existing research shows that local population and human capital composition, as well as selective out-migration, are important determinants of how severely local labor markets respond to industrial shocks (Coulomb and Zylberberg, 2021; Gagliardi et al., 2023; Fluegge, 2025; Krause, 2026b). The closure penalty documented here provides the variation on which the location choice framework in the next subsection builds.

RECOVERING AMENITY EFFECTS FROM SPATIAL EQUILIBRIUM

The reduced-form results document two opposing local consequences of IRD shutdowns: air quality improvements on the one hand, and declines in income, employment, and housing prices on the other. Taken together, these movements do not admit a single interpretation. Housing prices decline despite cleaner air, and the affected population does not appear to relocate. To make sense of this configuration, I embed the reduced-form estimates in a location choice framework that, under a spatial equilibrium restriction, recovers the movement in non-market amenities consistent with observed changes in income, housing prices, and population. The model is a standard application of the Rosen-Roback framework (Rosen, 1974; Roback, 1982) and is directly adapted from Bartik et al. (2019). Quentel (2025) provides a recent application to the German context.

Consider an economy that consists of N neighborhoods denoted by n and is populated by a mass of L workers indexed by l. Location-specific individual utility is a function of neighborhood amenities (A_n), the consumption of housing (h) and a numéraire consumption good (c) as well as a location-specific taste shock (η_{ln}). Let the average price of housing and the wage rate in neighborhood n be p_n and w_n, respectively. Assuming that workers' utility is Cobb-Douglas and that every worker inelastically supplies one unit of labor in the neighborhood they live in, the workers' maximization problem reads

$$\begin{aligned} \max_{c,h}\ u_{ln} &= A_n \cdot h^{\alpha} \cdot c^{1-\alpha} \cdot \eta_{ln} \\ s.t.\ h \cdot p_n + c &= w_n. \end{aligned} \tag{4}$$

The solution to the above problem yields the indirect utility of living in neighborhood n[18]

$$U_{ln} = \frac{A_n w_n}{p_n^{\alpha}} \eta_{ln}. \tag{5}$$

Hence, the probability that a worker chooses neighborhood n over any neighborhood r is given by

$$\mathbb{P}\Big(\frac{A_n w_n}{p_n^{\alpha}} \eta_{ln} \geq \frac{A_r w_r}{p_r^{\alpha}} \eta_{lr}\Big) \qquad \forall\, r \neq n.$$

Assuming that the neighborhood-specific taste shocks are distributed according to a Fréchet distribution with shape parameter ϕ, i.e., $\eta_{ln} \sim F(\eta) = \exp(-\eta^{-\phi})$, the share of workers living in neighborhood n is given by

[18] Since the utility takes a standard Cobb-Douglas form, the solution to the consumer problem is straightforward. The full derivation is given in the appendix.

$$s_n = \frac{\left(\frac{A_n w_n}{p_n^\alpha}\right)^\phi}{\sum_{r=1}^N \left(\frac{A_r w_r}{p_r^\alpha}\right)^\phi}. \tag{6}$$

Recall that total population in the economy is equal to L, so that the population in neighborhood n is equal to $R_n = L \cdot s_n$. Substituting into (6) and taking the natural logarithm of the equation, we can solve for amenities in neighborhood n as a function of observables and amenities in other neighborhoods

$$\ln(A_n) = \frac{1}{\phi}\ln(R_n) + \alpha \ln(p_n) - \ln(w_n) - \frac{1}{\phi}\ln(L) + \frac{1}{\phi}\ln\left[\sum_{r=1}^N \left(\frac{A_r w_r}{p_r^\alpha}\right)^\phi\right]. \tag{7}$$

For estimation purposes, note that the total population L and the sum $\sum_{r=1}^N \left(\frac{A_r w_r}{p_r^\alpha}\right)^\phi$ vary across years, but not across grid cells. Hence, introducing a time dimension and subsuming the two terms that are constant in cross-section into c_t, Equation (7) can be written as

$$\ln(A_{nt}) = \frac{1}{\phi}\ \ln(R_{nt}) + \alpha\ \ln(p_{nt}) - \ln(w_{nt}) + c_t. \tag{8}$$

Equation (8) expresses amenities as a function of observed variables, a time-variant term absorbed by the fixed effects in the empirical application, and the parameters ϕ and α. The model is specified in terms of the wage rate w_n, which I do not observe at the grid cell level and proxy by disposable household income per adult. This is arguably an imperfect mapping because disposable household income includes transfers and capital income and is net of taxes, so it does not isolate the price of labor that enters the model.[19] Nonetheless, it appears reasonable to assume that an important shock to local wages materializes in disposable income (although the raw wage response may be muted by tax-and-transfer systems). Population R_{nt} is observed directly as the adult population at the grid cell level. Housing prices p_{nt} are measured as the average listing price for houses, so that the amenity index can be constructed only for grid cell-years with at least one recorded house listing.

[19]The proxy is also imperfect along a second dimension. The model assumes that workers earn wages in their location of residence, whereas at the 1 km resolution commuting across cells is the norm. The relevant object captured by my measure is therefore the disposable income that residents of cell n obtain given their commuting options, rather than a wage paid in cell n itself.

The Fréchet shape parameter ϕ governs the dispersion of the taste shock and is commonly interpreted as a mobility elasticity: lower values increase the mass in the tail of the distribution, raising the probability that a worker chooses a neighborhood dominated on observables. I follow Quentel (2025), who calibrates $\phi = 4.56$ for the German context based on Krebs and Pflüger (2023).[20] Ahlfeldt et al. (2015) estimate a slightly higher mobility elasticity, which motivates alternative parameter choices in Table 2. As for α, the income share spent on housing, the range of parameters used in the literature varies considerably. Monte et al. (2018) argue for a comparatively high expenditure share of 0.4. Quentel (2025) estimates expenditure shares of 0.25 and 0.29 for high- and low-skilled residents respectively based on the German Microcensus. I thus compute amenities for a range of values between 0.2 and 0.4 to assess the robustness of the results to the choice of this parameter.

Equation (8) can now be used to estimate the effect of facility closures on amenities in neighborhoods experiencing an IRD closure. Using the static analogue of the event study methodology from above, I estimate the following equation

$$\ln(A_{nt}) = (\theta + \gamma \text{IndEmpl}_n) \cdot \mathbb{1}[t \geq \tau_n] + \mu_n + \omega_t + \epsilon_{nt} \tag{9}$$

where $\ln(A_{nt})$ is computed as in Equation (8) for a range of parameter values and c_t is contained in ω_t. Because $\ln(A_{nt})$ is a linear combination of the outcome variables analyzed above, this exercise introduces no new variation and its contribution is interpretive. The Cobb-Douglas preferences fix the weights on housing prices and income, while the sorting condition determines the weight on population and is what renders population informative about amenities. Under this structure, the weighted combination recovers the non-market component of location value. The heterogeneity structure mirrors Equation (3). Therefore, if the closure penalty documented above extends beyond the labor market, it should appear in γ. The results for different values of α and ϕ are shown in Table 2.

Table 2 confirms the pattern that the closure penalty would predict. Consistent with the reduced-form results, the baseline ATT for low-industrial neighborhoods is consistently insignificant, while neighborhoods with high baseline industrial employment experience a sig-

[20] Krebs and Pflüger (2023) estimate this parameter as a commuting elasticity in a richer spatial framework with both commuting and migration margins. In the absence of an estimate of pure migration elasticity at this resolution, I follow recent applications of the Bartik et al. (2019) framework in adopting this value, and assess the sensitivity of the results to alternative choices below.

Table 2: Effect of IRD Closure on Neighborhood Amenities

Dependent Variable:	Log Amenity Index		
Housing share parameter:	$\alpha = 0.2$	$\alpha = 0.3$	$\alpha = 0.4$
Panel A: Low Mobility Elasticity ($\phi = 2$)			
Closure	0.0009	0.0002	-0.0005
	(0.0043)	(0.0048)	(0.0054)
Closure $\times$ Industrial	-0.0114*	-0.0184***	-0.0255***
	(0.0058)	(0.0070)	(0.0082)
Panel B: Baseline Mobility Elasticity ($\phi = 4.56$)			
Closure	0.0005	-0.0002	-0.0009
	(0.0039)	(0.0044)	(0.0049)
Closure $\times$ Industrial	-0.0058	-0.0128**	-0.0199***
	(0.0048)	(0.0058)	(0.0070)
Panel C: High Mobility Elasticity ($\phi = 6$)			
Closure	0.0004	-0.0003	-0.0010
	(0.0039)	(0.0043)	(0.0049)
Closure $\times$ Industrial	-0.0047	-0.0118**	-0.0188***
	(0.0046)	(0.0056)	(0.0068)
Fixed Effects			
Year	✓	✓	✓
Grid Cell	✓	✓	✓
Observations	94,060	94,060	94,060

Clustered standard errors (Municipality) in parentheses.
*Signif. Codes: ***: 0.01, **: 0.05, *: 0.1*

Note: The table displays ATT estimates across all post-treatment periods for the effect of IRD closures on local amenities (in logs) as specified in Equation (9). The different panels display results for varying values of ϕ and columns show results for varying values of α. Amenities are computed as in Equation (8). The sample consists of all grid cells within a 5 km radius around closing IRD plants that record house listings. Standard errors are clustered by municipality.

nificant decline in the local amenity index following IRD shutdowns. The result is robust across alternative values of the housing expenditure share (α) and the mobility elasticity (ϕ). The amenity index recovered from Equation (8) reflects the non-market component of location value implied by the observed movements in income, housing prices, and population. In high-industrial neighborhoods, the air quality gains documented above are more than offset by deterioration along other dimensions of local quality, consistent with urban blight or the loss of economic activity historically anchored by the industrial site.

The Rosen-Roback framework interprets the absence of a population response through the joint movement of prices and income. The housing price decline in industrially dependent neighborhoods is large enough that, at conventional expenditure shares, the reduction in housing costs more than offsets the fall in nominal income (see Appendix F; Notowidigdo, 2020). Had local amenities remained constant, these neighborhoods would have become *more* attractive on net, and population should have grown. The absence of any population response therefore reveals a deterioration in non-market amenities sufficient to absorb the difference. Cheap housing, on this reading, compensates the marginal resident not for lower income alone, but also for living in a place that has become worse.

It is important to note that the model does not distinguish between renters and homeowners. In reality, incumbent homeowners absorb the same price decline that equalizes utility in the model as a capital loss on housing wealth. Thus, in practice, the model's compensation channel does not operate for these households. Additionally, even for renters, the channel hinges on the assumption of no moving costs, an assumption that abstracts from multiple factors that might drive people to stay in a declining area, and from the relatively short horizon of the data.

In summary, the model's spatial equilibrium logic equalizes utility for the marginal mobile worker, but the locality itself has shifted to a worse configuration where residents are nominally poorer and remain in less desirable places. The housing price decline that offsets these components is itself a wealth loss for incumbent owners. From a place-based perspective, this constitutes decline rather than a net welfare gain for host communities. The removal of an industrial polluter therefore does not automatically generate a green dividend for the surrounding area, and the amenity declines documented here make a case for targeted place-based policy, at least over the short horizon that the data can speak to.

VI CONCLUSION

Industrial and decarbonization policies are typically designed and evaluated at the national or supranational level. As this paper demonstrates, however, their welfare consequences can differ sharply across the neighborhoods that host the affected facilities.

By linking facility closures to socioeconomic conditions, housing markets, and air quality on a common 1km $\times$ 1km grid, I provide granular evidence on the local trade-offs inherent in large-scale industrial shutdowns. This paper shows that removing an industrial pollution source can induce adverse local labor market shocks that leave host communities worse off at least in the short run. This result is particularly stark for neighborhoods with a comparatively important industrial base at the time of the closure.

These findings have direct implications for the political economy of the green transition and structural change more broadly. The removal of a negative production externality does not automatically generate a net benefit for host communities, and structural change risks exacerbating local inequality even when it entails real environmental benefits. While industrial closures contribute to a reduction of the PM2.5 exposure gap across the income distribution, they also lead to a devaluation of local housing wealth and reductions in disposable household income in affected neighborhoods. From a regional inequality standpoint, environmental mandates are therefore likely to require complementary place-based economic policies to prevent regional decline in the most exposed areas (Hanson, 2023; Krause, 2026a).

These conclusions are drawn from a reduced-form analysis of local partial equilibrium effects over a comparatively short horizon. While I identify significant transitional costs for incumbent residents, a full accounting of the aggregate welfare effects is beyond the scope of this paper. Such an accounting would need to incorporate the global benefits of CO_2 abatement via the social cost of carbon, model the dispersion of avoided emissions beyond the immediate vicinity of closing plants, and capture the general equilibrium reallocation of labor and capital across sectors and space. Future structural work integrating these dimensions is needed to weigh the local distributional losses documented here against the broader societal gains of the green transition. The grid-cell data also leave open a question of incidence. Worker-level studies recover the earnings losses of displaced workers, but scaling such estimates to the loss sustained by a place presumes that incumbent workers are the only affected group. By linking closures to geolocalized worker-level records, future research could quantify the distribution of the place-based losses documented here across directly displaced workers and other residents affected through spillovers.

References

Ahlfeldt, G. M., Redding, S. J., Sturm, D. M., and Wolf, N. (2015). The Economics of Density: Evidence From the Berlin Wall. *Econometrica*, 83(6):2127–2189.

Ash, M. and Boyce, J. K. (2018). Racial Disparities in Pollution Exposure and Employment at US Industrial Facilities. *Proceedings of the National Academy of Sciences*, 115(42):10636–10641.

Balboni, C. and Shapiro, J. S. (2025). Spatial Environmental Economics. In Donaldson, D. and Redding, S. J., editors, *Handbook of Regional and Urban Economics*, volume 6, pages 585–652. Elsevier.

Banzhaf, H. S. (2021). Difference-in-Differences Hedonics. *Journal of Political Economy*, 129(8):2385–2414.

Banzhaf, H. S., Ma, L., and Timmins, C. (2019). Environmental Justice: Establishing Causal Relationships. *Annual Review of Resource Economics*, 11(1):377–398.

Banzhaf, H. S. and Walsh, R. P. (2008). Do People Vote with Their Feet? An Empirical Test of Tiebout. *American Economic Review*, 98(3):843–863.

Barreto, C., Grundke, R., and Krill, Z. (2023). The Cost of Job Loss in Carbon-intensive Sectors: Evidence from Germany. *OECD Economics Department Working Papers No. 1774*.

Bartik, A. W., Currie, J., Greenstone, M., and Knittel, C. R. (2019). The Local Economic and Welfare Consequences of Hydraulic Fracturing. *American Economic Journal: Applied Economics*, 11(4):105–155.

Bauer, T. K., Braun, S. T., and Kvasnicka, M. (2017). Nuclear Power Plant Closures and Local Housing Values: Evidence from Fukushima and the German Housing Market. *Journal of Urban Economics*, 99:94–106.

Bayer, P., McMillan, R., Murphy, A., and Timmins, C. (2016). A Dynamic Model of Demand for Houses and Neighborhoods. *Econometrica*, 84(3):893–942.

Bell, M. L. and Ebisu, K. (2012). Environmental Inequality in Exposures to Airborne Particulate Matter Components in the United States. *Environmental Health Perspectives*, 120(12):1699–1704.

Borusyak, K., Jaravel, X., and Spiess, J. (2024). Revisiting Event-Study Designs: Robust and Efficient Estimation. *Review of Economic Studies*, 91(6):3253–3285.

Bos, B., Drupp, M. A., and Sager, L. (2025). The Distributional Effects of Low Emission Zones: Who Benefits from Cleaner Air? *CESifo Working Paper 11739/ 2025*.

Breidenbach, P. and Eilers, L. (2018). RWI-GEO-GRID: Socio-Economic Data on Grid Level. *Jahrbücher für Nationalökonomie und Statistik*, 238(6):609–616.

Bruns, D. and Thomsen, S. L. (2025). The Impact of Germany's Coal Phase-Out on Local Property Values. In *VfS Annual Conference 2025 (Cologne): Revival of Industrial Policy*, number 325450. Verein für Socialpolitik/German Economic Association.

Bundesinstitut für Bau-, Stadt- und Raumforschung (BBSR) (2025). INKAR – Indikatoren und Karten zur Raum- und Stadtentwicklung. Laufende Raumbeobachtung des BBSR. Available at: https://www.inkar.de (Accessed: January 3, 2025).

Bundeskartellamt (2015). Case Report: Clearance of the Merger Between Immowelt and Immonet (File No. B6-39/15). Case report, Federal Cartel Office (Bundeskartellamt), Bonn.

Champalaune, P. (2026). Cleaner Air for Whom? Air Quality Policy and Persistent Exposure Disparities. *Working Paper*.

Chay, K. and Greenstone, M. (2005). Does Air Quality Matter? Evidence from the Housing Market. *Journal of Political Economy*, 113(2):376–424.

Colmer, J., Hardman, I., Shimshack, J., and Voorheis, J. (2020). Disparities in $PM_{2.5}$ Air Pollution in the United States. *Science*, 369(6503):575–578.

Colmer, J., Krause, E., Lyubich, E., and Voorheis, J. (2024). Transitional Costs and the Decline of Coal: Worker-Level Evidence. *Center for Economic Studies Working Paper 24-53*.

Coulomb, R. and Zylberberg, Y. (2021). Environmental Risk and the Anchoring Role of Mobility Rigidities. *Journal of the Association of Environmental and Resource Economists*, 8(3):509–542.

Currie, J., Davis, L., Greenstone, M., and Walker, R. (2015). Environmental Health Risks and Housing Values: Evidence from 1,600 Toxic Plant Openings and Closings. *American Economic Review*, 105(2):678–709.

Currie, J., Voorheis, J., and Walker, R. (2023). What Caused Racial Disparities in Particulate Exposure to Fall? New Evidence from the Clean Air Act and Satellite-Based Measures of Air Quality. *American Economic Review*, 113(1):71–97.

Davis, L. W. (2011). The Effect of Power Plants on Local Housing Values and Rents. *The Review of Economics and Statistics*, 93(4):1391–1402.

de Chaisemartin, C. and D'Haultfœuille, X. (2020). Two-Way Fixed Effects Estimators with Heterogeneous Treatment Effects. *American Economic Review*, 110(9):2964–2996.

Depro, B., Timmins, C., and O'Neil, M. (2015). White Flight and Coming to the Nuisance: Can Residential Mobility Explain Environmental Injustice? *Journal of the Association of Environmental and Resource Economists*, 2(3):439–468.

European Environment Agency (2018). Analysis of Air Pollution and Noise and Social Deprivation. *Eionet Report - ETC/ACM 2018/7*.

European Environment Agency (2024). The Costs to Health and the Environment from Industrial Air Pollution in Europe – 2024 Update. Briefing 24/2023, European Environment Agency, Copenhagen, Denmark.

Fairburn, J., Schüle, S. A., Dreger, S., Hilz, L. K., and Bolte, G. (2019). Social Inequalities in Exposure to Ambient Air Pollution: A Systematic Review in the WHO European Region. *International Journal of Environmental Research and Public Health*, 16(17):3127.

Fluegge, R. B. (2025). Death, Destruction, and Growth in Cities: Entrepreneurial Capital and Economic Geography after the 1918 Influenza. *Journal of Urban Economics*, 150:103810.

Fowlie, M., Rubin, E., and Walker, R. (2019). Bringing Satellite-Based Air Quality Estimates Down to Earth. *AEA Papers and Proceedings*, 109:283–288.

Fraenkel, R., Graff Zivin, J., and Krumholz, S. (2024). The Coal Transition and Its Implications for Health and Housing Values. *Land Economics*, 100(1):51–65.

Freeman, R., Liang, W., Song, R., and Timmins, C. (2019). Willingness to Pay for Clean Air in China. *Journal of Environmental Economics and Management*, 94:188–216.

Gagliardi, L., Moretti, E., and Serafinelli, M. (2023). The World's Rust Belts: The Heterogeneous Effects of Deindustrialization on 1,993 Cities in Six Countries. Working Paper 31948, National Bureau of Economic Research, Cambridge, MA.

Gamper-Rabindran, S. and Timmins, C. (2011). Hazardous Waste Cleanup, Neighborhood Gentrification, and Environmental Justice: Evidence from Restricted Access Census Block Data. *American Economic Review*, 101(3):620–624.

Gamper-Rabindran, S. and Timmins, C. (2013). Does Cleanup of Hazardous Waste Sites Raise Housing Values? Evidence of Spatially Localized Benefits. *Journal of Environmental Economics and Management*, 65(3):345–360.

Gardner, J., Thakral, N., Tô, L. T., and Yap, L. (2024). Two-Stage Differences in Differences. *Working Paper*.

Genesove, D. and Mayer, C. (2001). Loss Aversion and Seller Behavior: Evidence from the Housing Market. *The Quarterly Journal of Economics*, 116(4):1233–1260.

Germani, A. R., Morone, P., and Testa, G. (2014). Environmental Justice and Air Pollution: A Case Study on Italian Provinces. *Ecological Economics*, 106:69–82.

Goodman-Bacon, A. (2021). Difference-in-differences with Variation in Treatment Timing. *Journal of Econometrics*, 225(2):254–277.

Gornig, M. and Goebel, J. (2018). Deindustrialisation and the Polarisation of Household Incomes: The Example of Urban Agglomerations in Germany. *Urban Studies*, 55(4):790–806.

Graff Zivin, J. S. and Singer, G. (2022). Disparities in Pollution Capitalization Rates: The Role of Direct & Systemic Discrimination. Working Paper 30814, National Bureau of Economic Research, Cambridge, MA.

Grainger, C. A. (2012). The Distributional Effects of Pollution Regulations: Do Renters Fully Pay for Cleaner Air? *Journal of Public Economics*, 96(9-10):840–852.

Greenstone, M. and Gallagher, J. (2008). Does Hazardous Waste Matter? Evidence from the Housing Market and the Superfund Program. *Quarterly Journal of Economics*, 123(3):951–1003.

Haninger, K., Ma, L., and Timmins, C. (2017). The Value of Brownfield Remediation. *Journal of the Association of Environmental and Resource Economists*, 4(1):197–241.

Hanson, G. (2023). Local Labor Market Impacts of the Energy Transition: Prospects and Policies. Working Paper 30871, National Bureau of Economic Research, Cambridge, MA.

Haywood, L., Janser, M., and Koch, N. (2024). The Welfare Costs of Job Loss and Decarbonization: Evidence from Germany's Coal Phaseout. *Journal of the Association of Environmental and Resource Economists*, 11(3):577–611.

Heblich, S., Trew, A., and Zylberberg, Y. (2021). East-Side Story: Historical Pollution and Persistent Neighborhood Sorting. *Journal of Political Economy*, 129(5):1508–1552.

Henger, R. and Voigtländer, M. (2014). Transaktions-und Angebotsdaten von Wohnimmobilien. Eine Analyse für Hamburg. *IW-Trends-Vierteljahresschrift zur empirischen Wirtschaftsforschung*, 41(4):85–100.

Hernandez-Cortes, D. and Meng, K. C. (2023). Do Environmental Markets Cause Environmental Injustice? Evidence from California's Carbon Market. *Journal of Public Economics*, 217:104786.

Holland, S. P., Mansur, E. T., Muller, N. Z., and Yates, A. J. (2020). Decompositions and Policy Consequences of an Extraordinary Decline in Air Pollution from Electricity Generation. *American Economic Journal: Economic Policy*, 12(4):244–274.

Hsiang, S., Oliva, P., and Walker, R. (2019). The Distribution of Environmental Damages. *Review of Environmental Economics and Policy*, 13(1):83–103.

Jbaily, A., Zhou, X., Liu, J., Lee, T.-H., Kamareddine, L., Verguet, S., and Dominici, F. (2022). Air Pollution Exposure Disparities across US Population and Income Groups. *Nature*, 601(7892):228–233.

Jowers, K., Ma, Y., and Timmins, C. (2025). Costs of Exposure to Industrial Livestock Operations. *Land Economics*, 101(1):1–17.

Krause, E. (2026a). Adjusting to the Energy Transition: Training and Transfers in Coal Country. *Journal of Environmental Economics and Management*, 136:103264.

Krause, E. (2026b). Selective Migration and Regional Decline: Evidence from Coal Country. *Journal of Urban Economics*, 153:103858.

Krebs, O. and Pflüger, M. (2023). On the Road (again): Commuting and Local Employment Elasticities in Germany. *Regional Science and Urban Economics*, 99:103874.

Kuminoff, N. V. and Pope, J. C. (2014). Do "Capitalization Effects" for Public Goods Reveal the Public's Willingness to Pay? *International Economic Review*, 55(4):1227–1250.

Lavaine, E. (2015). An Econometric Analysis of Atmospheric Pollution, Environmental Disparities and Mortality Rates. *Environmental and Resource Economics*, 60(2):215–242.

Linn, J. (2013). The Effect of Voluntary Brownfields Programs on Nearby Property Values: Evidence from Illinois. *Journal of Urban Economics*, 78:1–18.

Miranda, M. L., Edwards, S. E., Keating, M. H., and Paul, C. J. (2011). Making the Environmental Justice Grade: The Relative Burden of Air Pollution Exposure in the United States. *International Journal of Environmental Research and Public Health*, 8(6):1755–1771.

Mohai, P., Pellow, D., and Roberts, J. T. (2009). Environmental Justice. *Annual Review of Environment and Resources*, 34(1):405–430.

Monte, F., Redding, S. J., and Rossi-Hansberg, E. (2018). Commuting, Migration, and Local Employment Elasticities. *American Economic Review*, 108(12):3855–3890.

Morehouse, J. M. and Rubin, E. (2026). Downwind and Out: The Strategic Dispersion of Power Plants and Their Pollution. *Journal of the Association of Environmental and Resource Economists*, 13(3):831–867.

Muehlenbachs, L., Spiller, E., and Timmins, C. (2015). The Housing Market Impacts of Shale Gas Development. *American Economic Review*, 105(12):3633–59.

Muñoz-Sabater, J., Dutra, E., Agustí-Panareda, A., Albergel, C., Arduini, G., Balsamo, G., Boussetta, S., Choulga, M., Harrigan, S., Hersbach, H., et al. (2021). ERA5-Land: A State-of-the-art Global Reanalysis Dataset for Land Applications. *Earth System Science Data*, 13(9):4349–4383.

Neier, T. (2021). Austrian Air – Just Clean for Locals: A Nationwide Analysis of Environmental Inequality. *Ecological Economics*, 187:107100.

Notowidigdo, M. J. (2020). The incidence of local labor demand shocks. *Journal of Labor Economics*, 38(3):687–725.

Quentel, M. (2025). Gone with the Wind: Renewable Energy Infrastructure, Welfare, and Redistribution. *Working Paper*.

Richardson, E. A., Pearce, J., Tunstall, H., Mitchell, R., and Shortt, N. K. (2013). Particulate Air Pollution and Health Inequalities: A Europe-wide Ecological Analysis. *International Journal of Health Geographics*, 12(1):34.

Roback, J. (1982). Wages, Rents, and the Quality of Life. *Journal of Political Economy*, 90(6):1257–1278.

Rosen, S. (1974). Hedonic Prices and Implicit Markets: Product Differentiation in Pure Competition. *Journal of Political Economy*, 82(1):34–55.

Rud, J.-P., Simmons, M., Toews, G., and Aragon, F. (2024). Job Displacement Costs of Phasing Out Coal. *Journal of Public Economics*, 236:105167.

RWI and Microm (2023). Socio-Economic Data on Grid Level - Scientific Use File (wave 13). doi: 10.7807/MICROM:SUF:V13 .

Rüttenauer, T. (2018). Neighbours Matter: A Nation-wide Small-Area Assessment of Environmental Inequality in Germany. *Social Science Research*, 70:198–211.

Sager, L. and Singer, G. (2025). Clean Identification? The Effects of the Clean Air Act on Air Pollution, Exposure Disparities, and House Prices. *American Economic Journal: Economic Policy*, 17(1):1–36.

Schaffner, S. and Thiel, P. (2024). FDZ Data description: Real-Estate Data for Germany (RWI-GEO-RED v10) – Advertisements on the Internet Platform ImmobilienScout24 2007-12/2023.

Schmieder, J. F., von Wachter, T., and Heining, J. (2023). The Costs of Job Displacement over the Business Cycle and Its Sources: Evidence from Germany. *American Economic Review*, 113(5):1208–54.

Umweltbundesamt (2023). Daten der Messnetze der Länder und des Umweltbundesamtes. https://www.umweltbundesamt.de/themen/luft/messenbeobachtenueberwachen/luftmessnetze-der-bundeslaender.

U.S. Environmental Protection Agency (2019). Integrated Science Assessment for Particulate

Matter. Final Report EPA/600/R-19/188, U.S. Environmental Protection Agency, Washington, DC.

van Donkelaar, A., Hammer, M. S., Bindle, L., Brauer, M., Brook, J. R., Garay, M. J., Hsu, N. C., Kalashnikova, O. V., Kahn, R. A., Lee, C., Levy, R. C., Lyapustin, A., Sayer, A. M., and Martin, R. V. (2021). Monthly Global Estimates of Fine Particulate Matter and Their Uncertainty. *Environmental Science & Technology*, 55(22):15287–15300.

vom Berge, P. and Schmillen, A. (2023). Effects of Mass Layoffs on Local Employment—Evidence from Geo-Referenced Data. *Journal of Economic Geography*, 23(3):509–539.

Supplemental Appendix

For Online Publication

Is There a Local Green Dividend? Evidence from Industrial Shutdowns in Germany

Philipp Bothe

August 2026

UTILITY MAXIMIZATION PROBLEM

The utility maximization problem of a worker in neighborhood n is given in Equation (4):

$$\max_{c,h} \; u_{ln} = A_n \cdot h^{\alpha} \cdot c^{1-\alpha} \cdot \eta_{ln}$$
$$s.t. \; h \cdot p_n + c = w_n.$$

The Lagrangian then writes

$$\mathcal{L} = A_n \cdot h^{\alpha} \cdot c^{1-\alpha} \cdot \eta_{ln} + \lambda(w_n - h \cdot p_n - c) \tag{10}$$

and the FOCs are given by

$$\frac{\partial \mathcal{L}}{\partial h} = \alpha A_n \eta_{ln} \left(\frac{c}{h}\right)^{1-\alpha} - \lambda p_n \overset{!}{=} 0 \tag{11}$$

$$\frac{\partial \mathcal{L}}{\partial c} = (1-\alpha) A_n \eta_{ln} \left(\frac{h}{c}\right)^{\alpha} - \lambda \overset{!}{=} 0 \tag{12}$$

$$\frac{\partial \mathcal{L}}{\partial \lambda} = w_n - h \cdot p_n - c \overset{!}{=} 0. \tag{13}$$

Dividing (11) by (12) and using the constraint yields the well-known expressions for optimal consumption under Cobb-Douglas preferences.

$$c = (1-\alpha)\, w_n \tag{14}$$

$$h = \alpha \, \frac{w_n}{p_n} \tag{15}$$

Substituting back into the utility function, we obtain the following expression for indirect utility

$$U_{ln} = \alpha^{\alpha}(1-\alpha)^{1-\alpha} \, \frac{A_n w_n}{p_n^{\alpha}} \eta_{ln}. \tag{16}$$

Since $\alpha^{\alpha}(1-\alpha)^{1-\alpha}$ is common across neighborhoods, it cancels from the choice probabilities and can be omitted, yielding Equation (5).

FIGURES

Figure A.1: Spatial Distribution of Mean Annual Particulate Matter Exposure in Germany

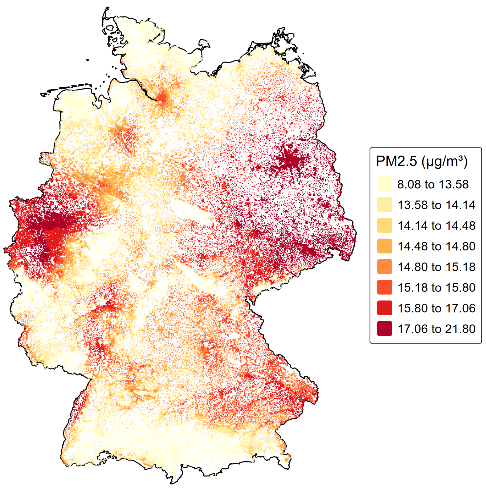

(a) Mean Ambient PM2.5, 2010

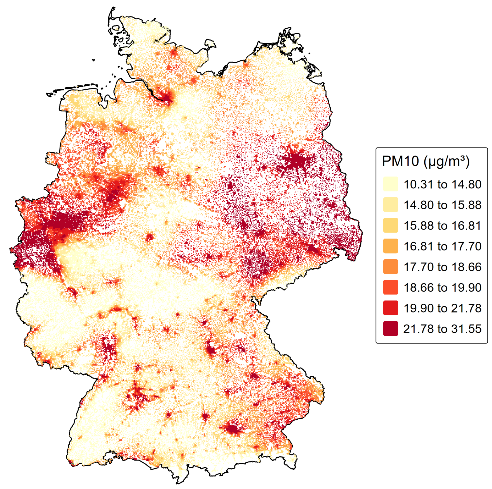

(b) Mean Ambient PM10, 2010

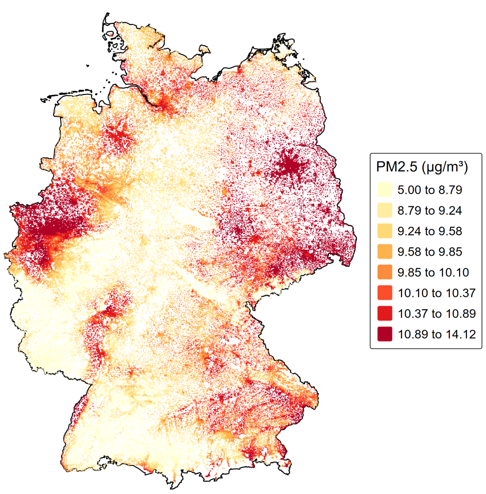

(c) Mean Ambient PM2.5, 2021

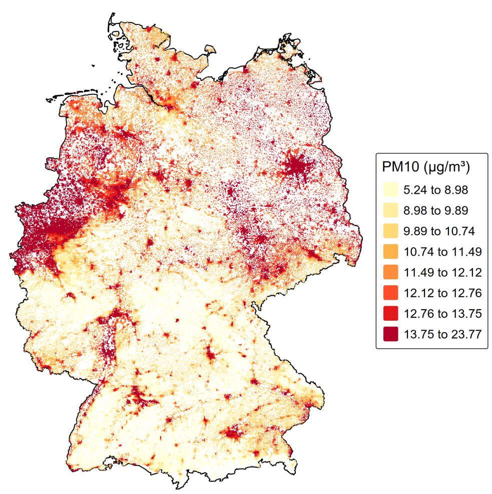

(d) Mean Ambient PM10, 2021

Note: The figure shows the average annual concentration of ambient $PM_{2.5}$ and PM_{10} by grid cell in Germany for 2010 (top row) and 2021 (bottom row). Particulate matter concentration is computed as the area-weighted mean of all pixels from the raster provided by van Donkelaar et al. (2021) and Umweltbundesamt (2023) respectively that overlap with a given grid cell. Unpopulated grid cells are excluded from the plot.

Figure A.2: Within-Municipality Distribution of PM2.5 for Berlin 2021

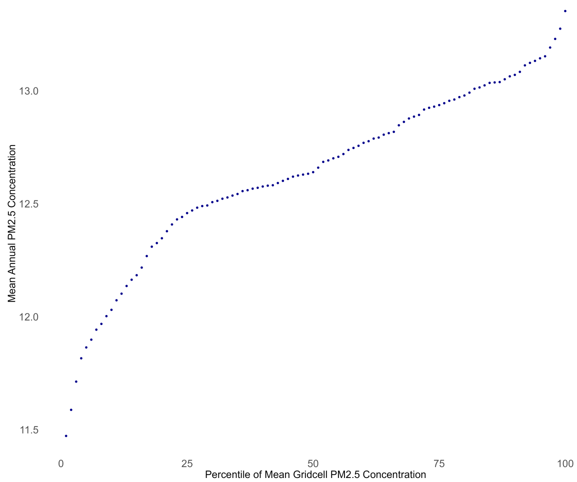

(a) PM2.5 Percentile

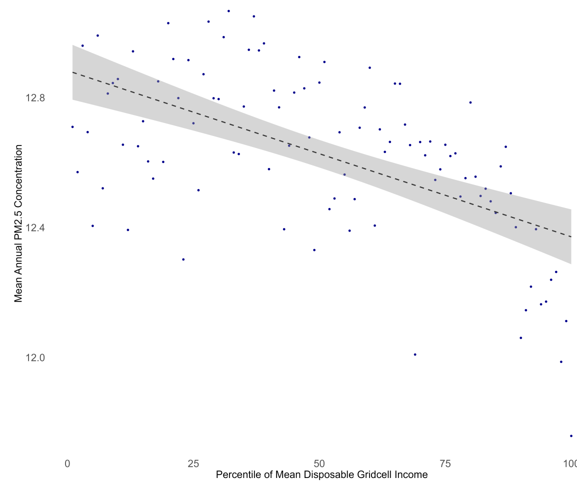

(b) Household Income Percentile

Note: The figure shows the mean PM2.5 exposure across population-weighted percentiles of the pollution distribution (a) and the household income distribution (b) within the municipality of Berlin in 2021. The dashed line in panel (b) represents the OLS fit of regressing the mean annual PM2.5 concentration on the household income percentile.

Figure A.3: Annual Mean PM2.5 Exposure Across the Grid Cell Income Distribution

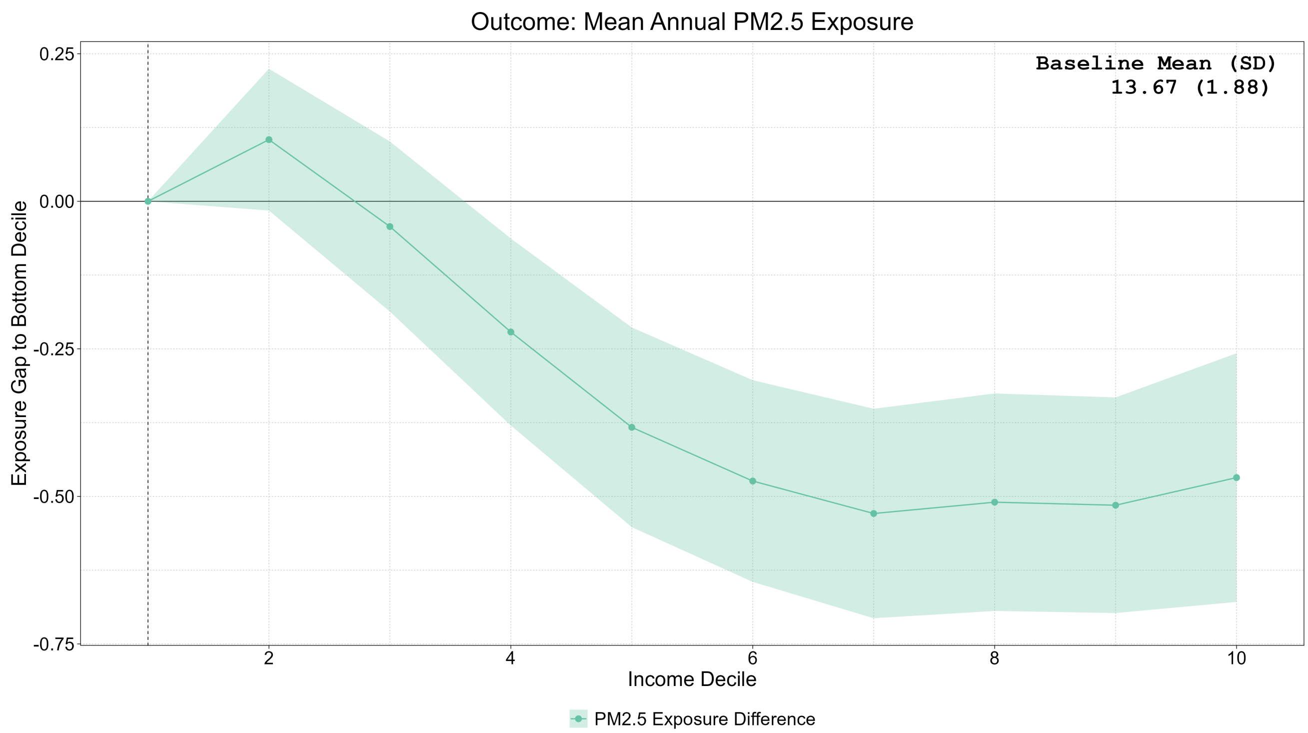

Note: The graph displays point estimates and 95% confidence intervals for ψ_k from Equation (1) estimated at the level of grid cells included in the estimation sample for the pre-treatment period 2010-2016. The outcome is mean ambient PM2.5 as measured by van Donkelaar et al. (2021). Estimates represent exposure differentials relative to the bottom decile. The model includes average annual temperature, daily precipitation and the magnitude of the mean wind vector. Standard errors are clustered by municipality. Regression outputs are reported in Table A.3.

Figure A.4: Annual Mean PM10 Exposure Across the Grid Cell Income Distribution

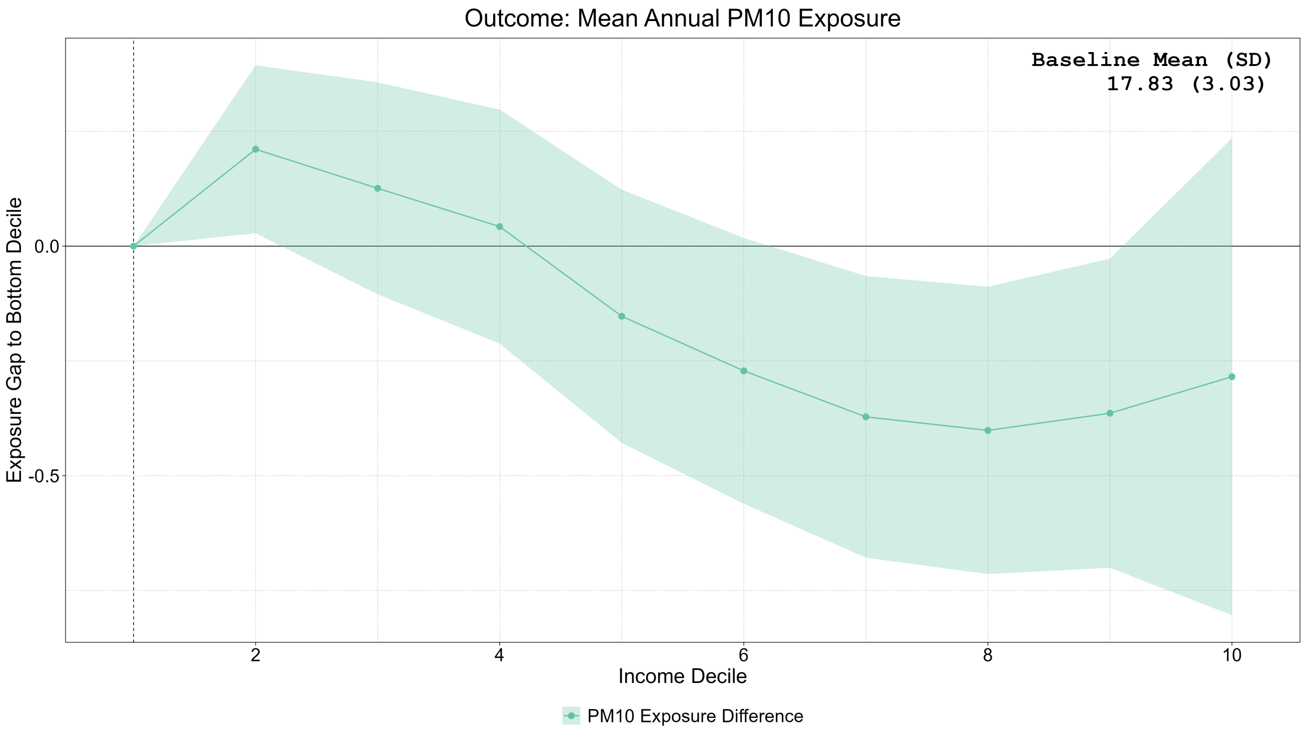

Note: The graph displays point estimates and 95% confidence intervals for ψ_k from Equation (1) estimated at the level of grid cells included in the estimation sample for the pre-treatment period 2010-2016. The outcome is mean ambient PM10 as measured by Umweltbundesamt (2023). Estimates represent exposure differentials relative to the bottom decile. The model includes mean annual temperature, average daily precipitation and the magnitude of the mean wind vector as controls. Standard errors are clustered by municipality. Regression outputs are reported in Table A.3.

Figure A.5: Location of Facility Closures in Germany

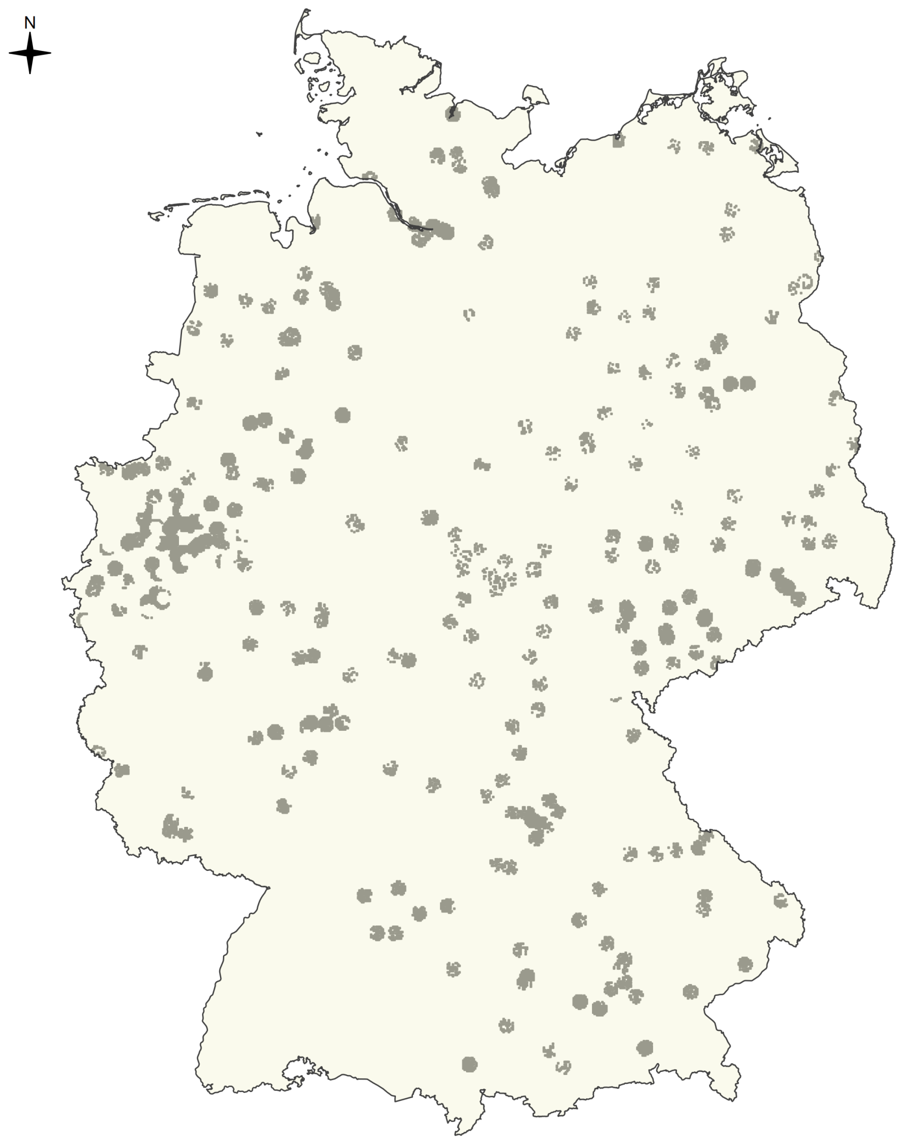

Note: The map shows the spatial distribution of plant closures in Germany across all years of the sample. Shaded areas indicate grid cells that are retained in the estimation sample as being within a 5 km radius around a closing plant.

Figure A.6: Pre-Treatment Evolution of Outcomes across Treatment Cohorts

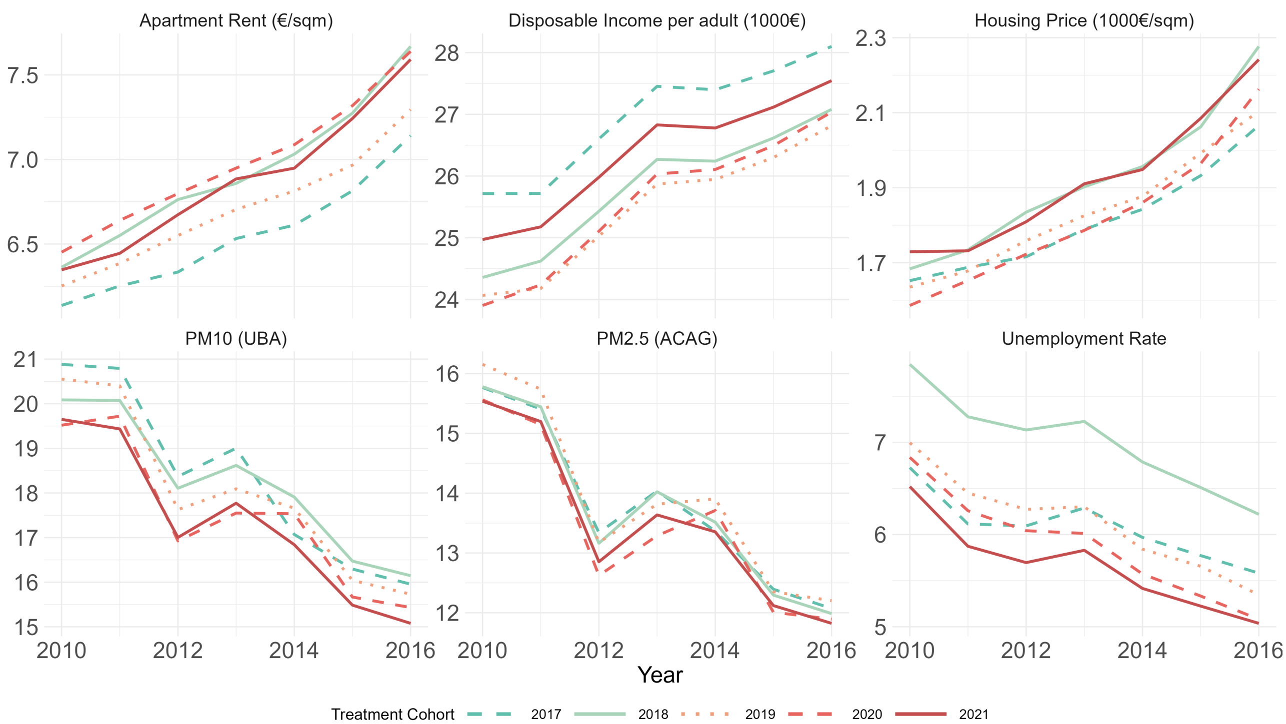

Note: The figure shows the evolution of all outcome variables used in the event study specification of Equation (2) over the common pre-treatment period 2010–2016, separately by treatment cohort. Cohorts are defined by the year of the first IRD closure affecting a given grid cell. Lines represent unweighted averages across all grid cells in a given cohort. The sample is restricted to grid cells within 5km of a closing IRD plant. PM2.5 (ACAG) refers to the satellite-based pollution measures by van Donkelaar et al. (2021). PM10 (UBA) refers to the monitor-based measure from Umweltbundesamt (2023).

Figure A.7: Effect of IRD Closure on Air Quality

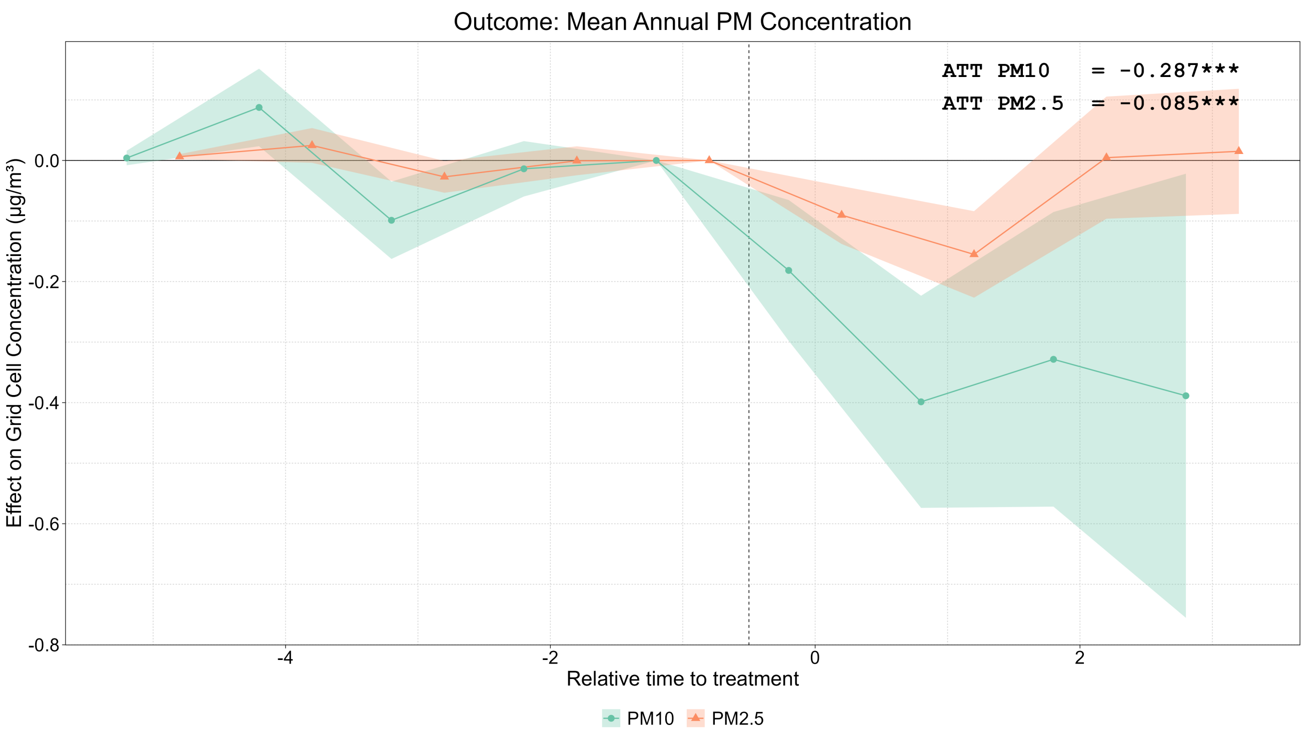

Note: The figure shows point estimates and 95% confidence intervals for θ_s from Equation (2). The outcome variable is the mean annual PM2.5 or PM10 concentration at the grid cell level as measured by van Donkelaar et al. (2021) and Umweltbundesamt (2023) respectively. Controls include mean temperature, average daily precipitation and the magnitude of the mean wind vector. The sample consists of all grid cells within a 5 km radius around plants that close down during the sample period and that fall within a single treatment buffer. Standard errors are clustered by municipality. The ATT estimates in the top right corner represent the joint effect across all post-treatment periods.

Figure A.8: Effect of IRD Closure on Adult Population (in logs)

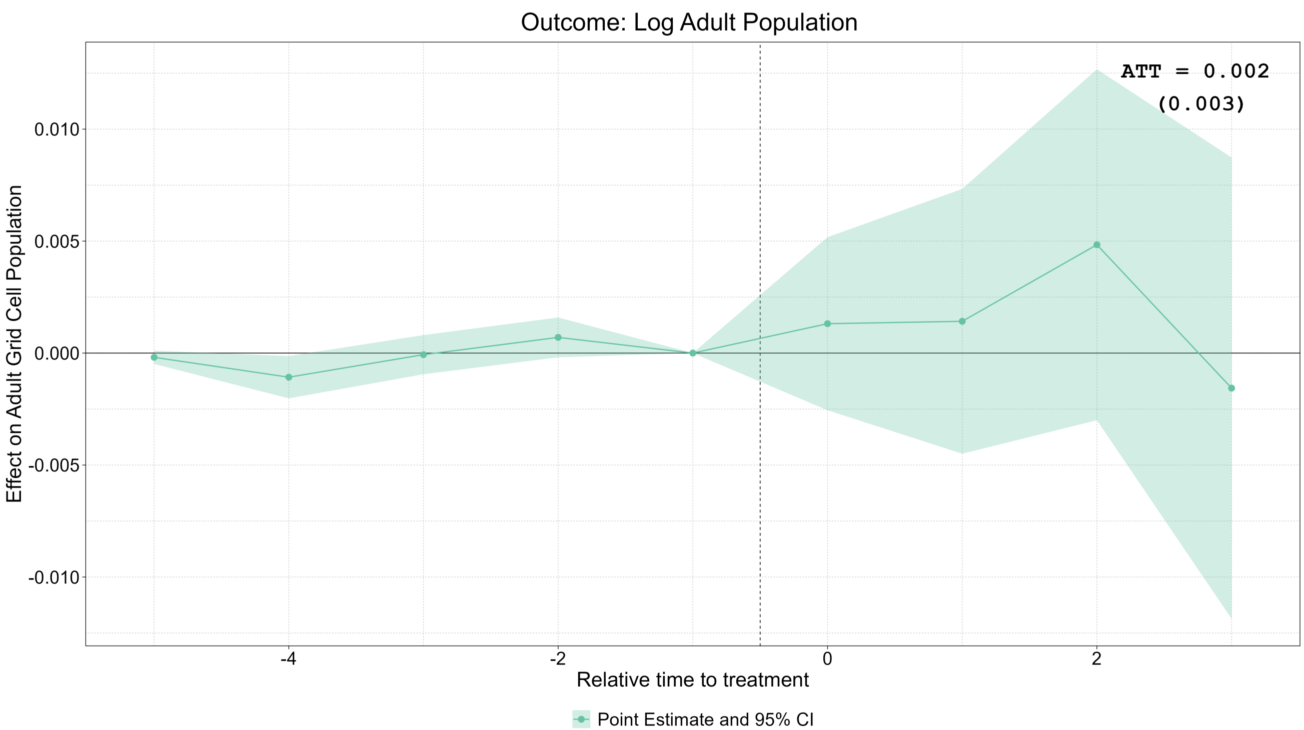

Note: The figure shows point estimates and 95% confidence intervals for θ_s from Equation (2). The outcome variable is the natural logarithm of adult population at the grid cell level. The sample consists of all grid cells within a 5 km radius around plants that close down during the sample period. Standard errors are clustered by municipality. The ATT estimate in the top right corner represents the joint effect across all post-treatment periods.

TABLES

Table A.1: Summary Statistics for Full and Estimation Sample

Variable	Mean	SD	P25	Median	P75
	Full Sample				
PM2.5 v Donkelaar ($\mu g/m^3$)	11.93	2.215	10.35	11.74	13.44
PM10 UBA ($\mu g/m^3$)	14.51	3.233	12.18	14.3	16.55
Disp HH Income (€ 1000 per adult)	26.29	4.587	23.2	25.85	28.86
Unemployment Rate (%)	4.741	3.285	2.47	3.96	6.16
Adult Population	456.7	1001	43.13	119.3	396
Industrial Employment (%)	17.93	6.668	12.94	17.21	21.95
Precipitation (mm/day)	2.399	0.5542	2.071	2.331	2.644
Temperature (°C)	9.752	1.144	9.069	9.871	10.54
Wind Vector Magnitude (m/s)	0.9125	0.4133	0.5982	0.8501	1.24
N	1,779,335				
	Estimation Sample				
PM2.5 v Donkelaar ($\mu g/m^3$)	12.69	2.229	11.25	12.57	14.23
PM10 UBA ($\mu g/m^3$)	16.72	3.388	14.26	16.5	19.1
Disp HH Income (€ 1000 per adult)	26.75	4.818	23.36	26.33	29.62
Unemployment Rate (%)	5.689	3.831	2.91	4.85	7.66
House Price (€ per m^2)	2127	1335	1360	1845	2530
Apartment Rent (€ per m^2)	7.347	2.538	5.614	6.727	8.419
Adult Population	999.4	1676	72.43	275.2	1176
Industrial Employment (%)	17.69	6.437	12.67	16.85	21.45
Precipitation (mm/day)	2.349	0.4515	2.076	2.33	2.604
Temperature (°C)	10.03	1.122	9.352	10.17	10.87
Wind Vector Magnitude (m/s)	0.9877	0.4137	0.6513	0.9741	1.332
N	179,933				

Note: The table shows summary statistics pooled across all years in the sample for the full sample of all populated areas of Germany (top panel) and the restricted estimation sample (bottom panel). The restricted sample excludes all grid cells located outside a 5km radius of closing IRD sites. The estimation sample reported here excludes observations from calendar year 2021 as there is no valid control group for units treated in 2021 but the cohort is used as valid control for all other units throughout.

Table A.2: Number of Grid Cells in Estimation Sample by E-PRTR Activity of Closed Facility

Code	Activity	Grid Cells	Share of Adult Pop. (%)
Energy industries			
1(b)	Gasification / liquefaction of fuels	45	0.05
1(c)	Combustion of fuels (other installations)	1,185	12.88
Production and processing of metals			
2(c)(iii)	Ferrous metals: protective fused metal coats	292	1.69
2(d)	Ferrous metal foundries	1,046	6.23
2(e)	Non-ferrous metals (production)	192	0.78
2(e)(ii)	Non-ferrous metals (smelting / refining)	682	2.65
2(f)	Surface treatment of metals and plastics	1,478	9.18
Mineral industry			
3(b)	Opencast mining and quarrying	177	0.77
3(c)(iii)	Cement clinker or lime (other furnaces)	33	0.04
3(e)	Manufacture of glass / glass fibre	131	1.42
3(g)	Manufacture of ceramic products	465	4.22
Chemical industry			
4(a)	Organic chemicals (general)	293	1.78
4(a)(i)	Simple hydrocarbons	35	0.11
4(a)(ii)	Oxygen-containing hydrocarbons	187	1.53
4(a)(vii)	Organometallic compounds	173	0.66
4(a)(viii)	Basic plastic materials	199	0.84
4(b)	Inorganic chemicals (general)	5	0.06
4(b)(iv)	Salts	25	0.06
4(b)(v)	Non-metals, metal oxides, other inorganic compounds	3	0.02
4(d)	Plant protection products and biocides	50	0.29
4(e)	Pharmaceutical products	120	0.83
4(f)	Explosives	84	0.21
Waste management			
5(a)	Disposal / recovery of hazardous waste	2,453	17.75
5(b)	Incineration of non-hazardous waste	105	0.61
5(c)	Disposal of non-hazardous waste	372	3.22
5(d)	Landfills	1,525	6.35
5(e)	Disposal / recovery of animal carcasses	30	0.18
5(f)	Urban waste-water treatment	80	0.20
5(g)	Independent waste-water treatment	16	0.20
Paper and wood production and processing			
6(b)	Production of paper, board, or pulp	203	0.59
6(c)	Preservation of wood and wood products	123	0.26
Intensive livestock and food			
7(a)(i)	Rearing of poultry	382	0.61
7(a)(ii)	Rearing of production pigs	445	0.51
7(a)(iii)	Rearing of sows	249	0.40
Food and beverage production			
8(a)	Slaughterhouses	185	0.35
8(b)(i)	Treatment of animal raw materials	97	0.23
8(b)(ii)	Treatment of vegetable raw materials	280	4.53
8(c)	Milk treatment and processing	152	0.31
Other activities			
9(a)	Pre-treatment or dyeing of fibres or textiles	8	0.03
9(c)	Surface treatment using organic solvents	881	7.46
9(d)	Production of carbon or electrographite	45	0.11
9(e)	Building / painting of ships	45	0.09
Total (in cross-section)		14,576	90.28

Note: The table reports the number of grid cells in the estimation sample, classified by the main activity code of the closing IRD facility that defines their treatment, together with the share of the estimation sample's adult population living in those cells. Codes follow Annex I of Regulation (EC) No 166/2006 (E-PRTR). Grid cells located within 5km of multiple closing facilities appear once classified by activity type of the facility that shuts down first. Activity codes are reported only for former E-PRTR plants, so the population shares do not sum to 100: the remaining 9.7% of the sample's adult population lives in the 1,892 grid cells whose closing facility carries no activity code. Population shares are computed from adult population averaged over the years each cell is observed.

Table A.3: Annual Particulate Matter Exposure Across the Grid Cell Income Distribution

	Estimation Sample		Full Sample	
Dependent Variables:	PM2.5	PM10	PM2.5	PM10
Model:	(1)	(2)	(3)	(4)
2nd Decile	0.1045*	0.2110**	-0.0937***	-0.1593***
	(0.0612)	(0.0932)	(0.0271)	(0.0294)
3rd Decile	-0.0428	0.1259	-0.3344***	-0.4535***
	(0.0735)	(0.1177)	(0.0347)	(0.0383)
4th Decile	-0.2215***	0.0425	-0.5050***	-0.6511***
	(0.0807)	(0.1299)	(0.0371)	(0.0435)
5th Decile	-0.3830***	-0.1527	-0.5546***	-0.7529***
	(0.0862)	(0.1405)	(0.0383)	(0.0475)
6th Decile	-0.4740***	-0.2716*	-0.5521***	-0.7758***
	(0.0871)	(0.1475)	(0.0396)	(0.0506)
7th Decile	-0.5290***	-0.3718**	-0.5182***	-0.7500***
	(0.0904)	(0.1563)	(0.0407)	(0.0547)
8th Decile	-0.5098***	-0.4014**	-0.4862***	-0.7116***
	(0.0939)	(0.1595)	(0.0416)	(0.0582)
9th Decile	-0.5150***	-0.3640**	-0.4621***	-0.6406***
	(0.0931)	(0.1716)	(0.0436)	(0.0674)
10th Decile	-0.4682***	-0.2843	-0.4642***	-0.5366***
	(0.1073)	(0.2648)	(0.0510)	(0.1053)
Fixed-effects & Controls				
Weather Controls	✓	✓	✓	✓
Year FE	✓	✓	✓	✓
Fit statistics				
Observations	114,187	114,075	1,779,335	1,777,684
R^2	0.62944	0.54589	0.73838	0.65628
Within R^2	0.24400	0.35549	0.16932	0.36008

Clustered standard errors (Municipality) in parentheses
*Signif. Codes: ***: 0.01, **: 0.05, *: 0.1*

Note: The table reports regression results obtained from estimating Equation (1) on the restricted pre-treatment estimation sample (Columns (1) and (2)) and the full sample for the entire area of Germany (Columns (3) and (4)). PM2.5 concentrations are obtained from van Donkelaar et al. (2021), PM10 concentrations from Umweltbundesamt (2023). Coefficients represent the mean annual exposure gap in $\mu g/m^3$ with respect to the bottom income decile. Income deciles are population-weighted and formed within year, and are identical across columns, so that the two pollutants are compared over the same set of grid cells. Weather controls include average temperature, daily precipitation and the magnitude of the mean wind vector. The PM10 columns rest on marginally fewer observations because PM10 is not reported for grid cells at the edge of the UBA raster. Magnitudes are not directly comparable across pollutants. Over the pre-treatment period the standard deviation of PM10 is 3.03 $\mu g/m^3$ against 1.88 $\mu g/m^3$ for PM2.5 (3.23 and 2.22 respectively in the full sample). Standard errors are clustered by municipality.

Table A.4: Effect of IRD Closure on House Prices and Apartment Rents

Dependent Variables:	House Prices			Apartment Rents		
Model:	(1)	(2)	(3)	(4)	(5)	(6)
Closure	-0.0156**	-0.0148*	-0.0274***	-0.0090	-0.0076	-0.0130*
	(0.0079)	(0.0088)	(0.0085)	(0.0065)	(0.0068)	(0.0071)
Single Treatment		✓			✓	
Year	✓	✓		✓	✓	
Year × Sector			✓			✓
Grid Cell	✓	✓	✓	✓	✓	✓
Observations	94,790	66,622	81,551	86,946	58,014	75,467
R^2	0.00050	0.00038	0.00166	0.00108	0.00066	0.00231
Adjusted R^2	0.00050	0.00038	0.00166	0.00108	0.00066	0.00231

Clustered standard errors (Municipality) in parentheses.
*Signif. Codes: ***: 0.01, **: 0.05, *: 0.1*

Note: The table shows ATT estimates for the effect of IRD closures on mean house prices (Columns (1) - (3)) and apartment rents (Columns (4) - (6)) at the grid cell level. Columns (1) and (4) show the effects for the full sample, i.e. all grid cells located within a 5km radius of a closing plant. Columns (2) and (5) show the results from a specification excluding grid cells located within 5km of *multiple* closing plants. Columns (3) and (6) show the results from a specification including sector-by-year fixed effects. Standard errors are clustered by municipality. Varying sample sizes are due to some grid cells not having any recorded listings in certain years.

Table A.5: Effect of IRD Closure on Disposable Household Income and Unemployment

Dependent Variables:	Income				Unemployment			
Model:	(1)	(2)	(3)	(4)	(5)	(6)	(7)	(8)
Closure	-0.0081***	-0.0063**	-0.0053*	-0.0048	0.0226	-0.0427	-0.0643	-0.0541
	(0.0026)	(0.0027)	(0.0030)	(0.0030)	(0.0622)	(0.0651)	(0.0711)	(0.0662)
Closure × Industrial		-0.0120***	-0.0051	-0.0166***		0.4752***	0.3786***	0.5193***
		(0.0043)	(0.0043)	(0.0044)		(0.1107)	(0.0909)	(0.0864)
Single Treatment			✓				✓	
Year	✓	✓	✓		✓	✓	✓	
Year × Sector				✓				✓
Grid Cell	✓	✓	✓	✓	✓	✓	✓	✓
Observations	179,933	178,495	134,551	152,330	179,933	178,495	134,551	152,330
R^2	0.00569	0.00768	0.00326	0.00841	8.71×10^{-5}	0.00652	0.00357	0.00832
Adjusted R^2	0.00569	0.00767	0.00325	0.00840	8.71×10^{-5}	0.00652	0.00356	0.00831

Clustered standard errors (Municipality) in parentheses.
*Signif. Codes: ***: 0.01, **: 0.05, *: 0.1*

Note: The table shows ATT estimates for the effect of IRD closures on log disposable household income per adult (Columns (1) - (4)) and the unemployment rate (Columns (5) - (8)) at the grid cell level. The first column for each outcome shows the aggregate treatment effect for both variables, the second column for each outcome shows the baseline effect and the interaction effect for grid cells with high baseline industrial employment. The third column for each outcome shows the results from a specification excluding grid cells located within 5km of multiple closing plants. The fourth column for each outcome shows the results from a specification including sector-by-year fixed effects. Standard errors are clustered by municipality.

B ROBUSTNESS CHECKS – 10KM BUFFER

Table B.1: Effect of IRD Closure on Air Quality

Dependent Variables:	PM2.5 (van Donkelaar)				PM10 (UBA)			
Model:	(1)	(2)	(3)	(4)	(5)	(6)	(7)	(8)
Closure	-0.1016***	-0.0918***	-0.0949***	-0.0910***	-0.2684***	-0.2584***	-0.2028***	-0.2813***
	(0.0201)	(0.0183)	(0.0218)	(0.0193)	(0.0582)	(0.0575)	(0.0588)	(0.0634)
Single Treatment			✓				✓	
Weather Controls		✓	✓	✓		✓	✓	✓
Year	✓	✓	✓		✓	✓	✓	
Year × Sector				✓				✓
Grid Cell	✓	✓	✓	✓	✓	✓	✓	✓
Observations	466,185	466,185	290,754	402,610	465,731	465,731	290,430	402,230
R^2	0.00628	0.00570	0.00485	0.00624	0.00831	0.00795	0.00433	0.01000
Adjusted R^2	0.00628	0.00570	0.00485	0.00624	0.00831	0.00795	0.00433	0.01000

Clustered standard errors (Municipality) in parentheses.
*Signif. Codes: ***: 0.01, **: 0.05, *: 0.1*

Note: The table shows ATT estimates for the effect of IRD closures on mean particulate matter concentration across all post-treatment periods for grid cells located within 10km of a closing IRD plant. Columns (1) - (4) report results using PM2.5 data provided by van Donkelaar et al. (2021) and columns (5) - (8) show results based on PM10 data from Umweltbundesamt (2023). Columns (3) and (7) exclude grid cells located within 10km of multiple closing plants. Reduced sample size in columns (4) and (8) is due to incomplete sector assignments at the facility level. Standard errors are clustered by municipality.

Table B.2: Effect of IRD Closure on Neighborhood Amenities

Dependent Variable:	Log Amenity Index		
Housing share parameter:	$\alpha = 0.2$	$\alpha = 0.3$	$\alpha = 0.4$
Panel A: Low Mobility Elasticity ($\phi = 2$)			
Closure	0.0097***	0.0080**	0.0064
	(0.0034)	(0.0037)	(0.0041)
Closure × Industrial	-0.0161***	-0.0224***	-0.0287***
	(0.0047)	(0.0054)	(0.0063)
Panel B: Baseline Mobility Elasticity ($\phi = 4.56$)			
Closure	0.0097***	0.0081**	0.0064*
	(0.0030)	(0.0033)	(0.0037)
Closure × Industrial	-0.0101**	-0.0163***	-0.0226***
	(0.0040)	(0.0047)	(0.0056)
Panel C: High Mobility Elasticity ($\phi = 6$)			
Closure	0.0097***	0.0081**	0.0064*
	(0.0029)	(0.0033)	(0.0037)
Closure × Industrial	-0.0089**	-0.0152***	-0.0215***
	(0.0040)	(0.0046)	(0.0055)
Fixed Effects Year	✓	✓	✓
Grid Cell	✓	✓	✓
Observations	220,697	220,697	220,697

Clustered standard errors (Municipality) in parentheses.
*Signif. Codes: ***: 0.01, **: 0.05, *: 0.1*

Note: The table displays ATT estimates across all post-treatment periods for the effect of IRD closures on local amenities (in logs) as specified in Equation (9). The different panels display results for varying values of ϕ and columns show results for varying values of α. Amenities are computed as in Equation (8). The sample includes all grid cells within a 10km radius of closing IRD sites that have recorded house listings. Standard errors are clustered by municipality.

Table B.3: Effect of IRD Closure on House Prices and Apartment Rents

Dependent Variables:	House Prices			Apartment Rents		
Model:	(1)	(2)	(3)	(4)	(5)	(6)
Closure	-0.0225***	-0.0108	-0.0312***	-0.0157***	-0.0121**	-0.0166***
	(0.0056)	(0.0072)	(0.0060)	(0.0045)	(0.0054)	(0.0050)
Single Treatment		✓			✓	
Year	✓	✓		✓	✓	
Year × Sector			✓			✓
Grid Cell	✓	✓	✓	✓	✓	✓
Observations	222,719	124,397	196,606	187,639	94,340	167,802
R^2	0.00104	0.00016	0.00209	0.00336	0.00146	0.00382
Adjusted R^2	0.00104	0.00016	0.00209	0.00336	0.00146	0.00382

Clustered standard errors (Municipality) in parentheses.
*Signif. Codes: ***: 0.01, **: 0.05, *: 0.1*

Note: The table shows ATT estimates for the effect of IRD closures on mean house prices (Columns (1) - (3)) and apartment rents (Columns (4) - (6)) at the grid cell level. Columns (1) and (4) show the effects for the full sample, i.e. all grid cells located within a 10km radius of a closing plant. Columns (2) and (5) show the results from a specification excluding grid cells located within 10km of *multiple* closing plants. Columns (3) and (6) show the results from a specification including sector-by-year fixed effects. Standard errors are clustered by municipality. Varying sample sizes are due to some grid cells not having any recorded listings in certain years.

Table B.4: Effect of IRD Closure on Disposable Household Income and Unemployment

Dependent Variables:	Income				Unemployment			
Model:	(1)	(2)	(3)	(4)	(5)	(6)	(7)	(8)
Closure	-0.0154***	-0.0144***	-0.0071***	-0.0146***	0.1478***	0.0989**	0.0084	0.0776
	(0.0018)	(0.0019)	(0.0019)	(0.0020)	(0.0455)	(0.0480)	(0.0599)	(0.0523)
Closure × Industrial		-0.0081**	-0.0030	-0.0112***		0.3717***	0.3580***	0.4792***
		(0.0034)	(0.0035)	(0.0032)		(0.0696)	(0.0723)	(0.0587)
Single Treatment			✓				✓	
Year	✓	✓	✓		✓	✓	✓	
Year × Sector				✓				✓
Grid Cell	✓	✓	✓	✓	✓	✓	✓	✓
Observations	466,185	462,346	288,242	399,535	466,185	462,346	288,242	399,535
R^2	0.02083	0.02216	0.00443	0.02530	0.00400	0.00779	0.00290	0.01032
Adjusted R^2	0.02083	0.02216	0.00443	0.02530	0.00400	0.00778	0.00290	0.01032

Clustered standard errors (Municipality) in parentheses.
*Signif. Codes: ***: 0.01, **: 0.05, *: 0.1*

Note: The table shows ATT estimates for the effect of IRD closures on log disposable household income per adult (Columns (1) - (4)) and the unemployment rate (Columns (5) - (8)) at the grid cell level. The first column for each outcome shows the aggregate treatment effect for both variables, the second column for each outcome shows the baseline effect and the interaction effect for grid cells with high baseline industrial employment. The third column for each outcome shows the results from a specification excluding grid cells located within 10km of multiple closing plants. The fourth column for each outcome shows the results from a specification with sector-by-year fixed effects. Standard errors are clustered by municipality.

Figure B.1: Pre-Treatment Evolution of Outcomes across Treatment Cohorts

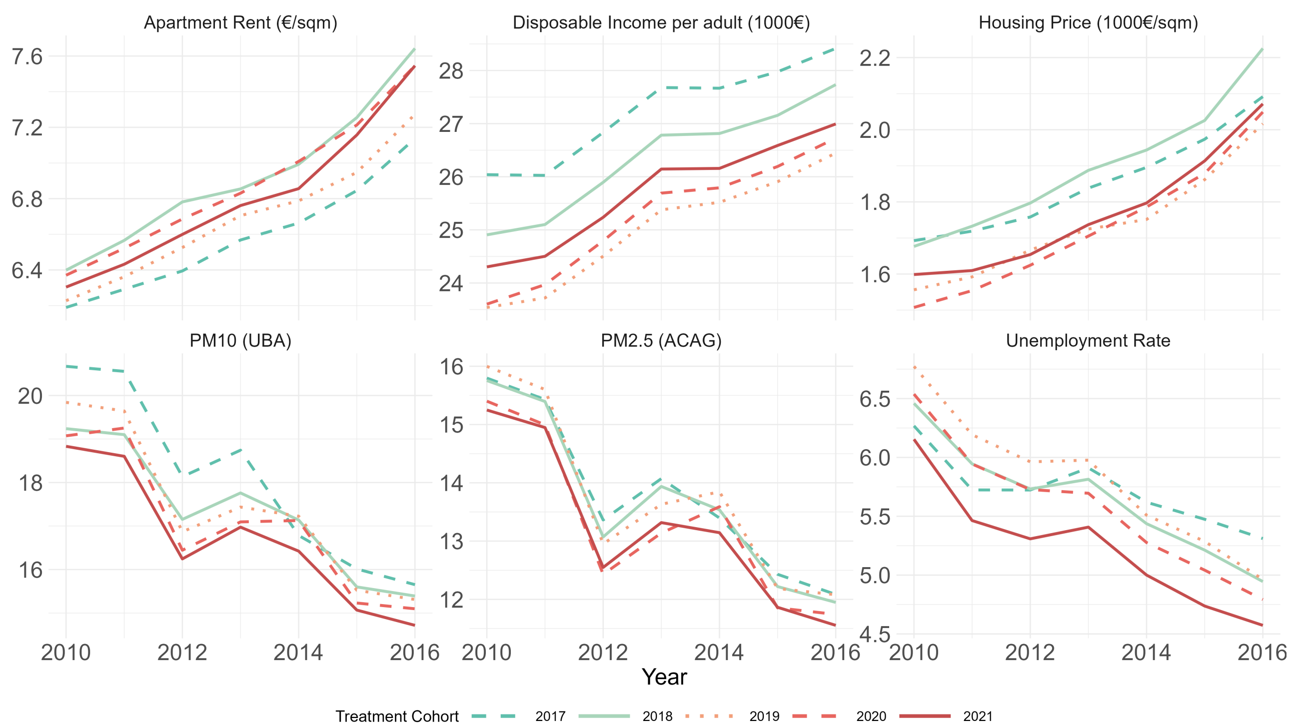

Note: The figure shows the evolution of all outcome variables used in the event study specification of Equation (2) over the common pre-treatment period 2010–2016, separately by treatment cohort. Cohorts are defined by the year of the first IRD closure affecting a given grid cell. Lines represent unweighted averages across all grid cells in a given cohort. The sample is restricted to grid cells within 10 km of a closing IRD plant. PM2.5 (ACAG) refers to the satellite-based pollution measures by van Donkelaar et al. (2021). PM10 (UBA) refers to the monitor-based measure from Umweltbundesamt (2023).

Figure B.2: Treatment Effect Heterogeneity for PM2.5 by Income Decile

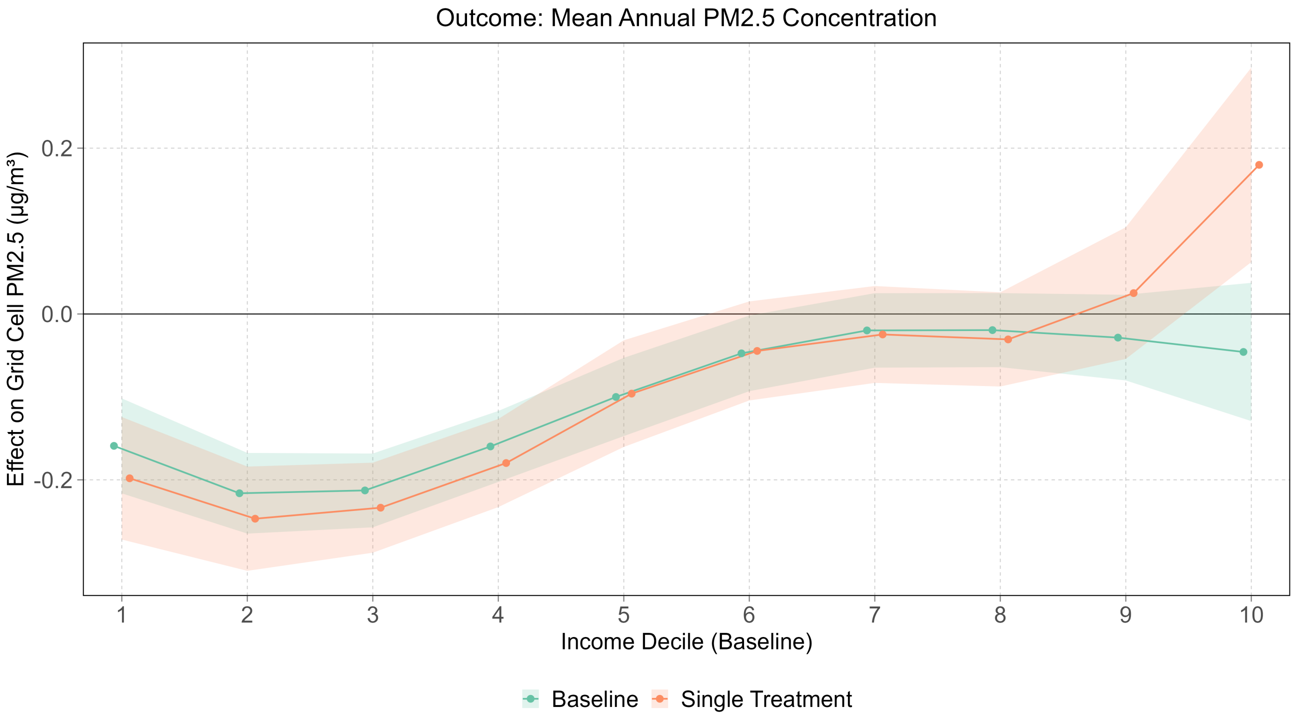

Note: The figure shows the average treatment effect and 95% confidence interval for the effect of an IRD shutdown on PM2.5 concentration in surrounding grid cells averaged across all post-treatment periods by baseline (pre-treatment) income decile of the treated grid cells. Estimates correspond to results obtained using the model from Equation (2) with treatment interacted with baseline income decile. Standard errors are clustered by municipality. Single Treatment refers to estimates obtained excluding grid cells located in the intersection of multiple treatment buffers.

Figure B.3: Effect of IRD Closure on House Prices and Apartment Rents

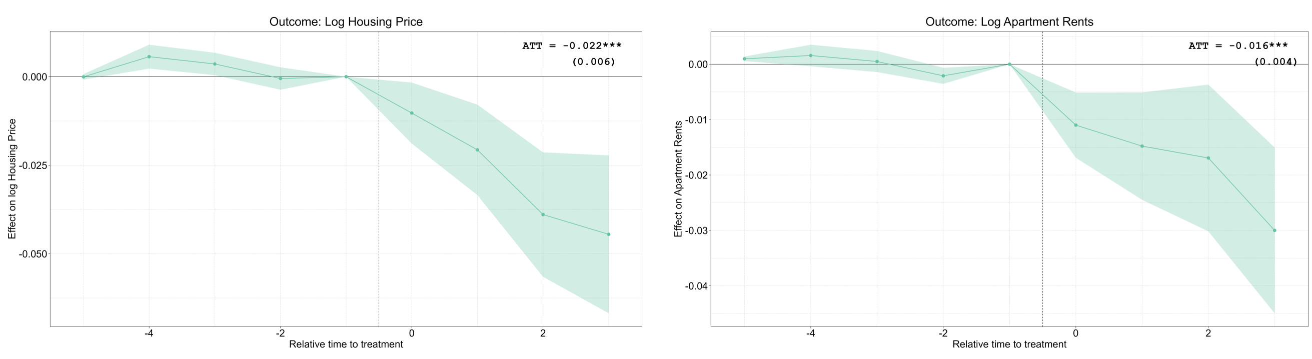

(a) House Prices (in logs)

(b) Apartment Rents (in logs)

Note: The figure shows point estimates and 95% confidence intervals for θ_s from Equation (2). The outcome variables are the natural logarithm of average house prices per square meter (Panel (a)) and average apartment rents per square meter (Panel (b)) at the grid cell level. The sample consists of all grid cells within a 10 km radius around plants that close down during the sample period. Standard errors are clustered by municipality. The ATT estimates in the top right corner of each panel represent the joint effect across all post-treatment periods.

Figure B.4: Effect of IRD Closure on Disposable Household Income and Unemployment

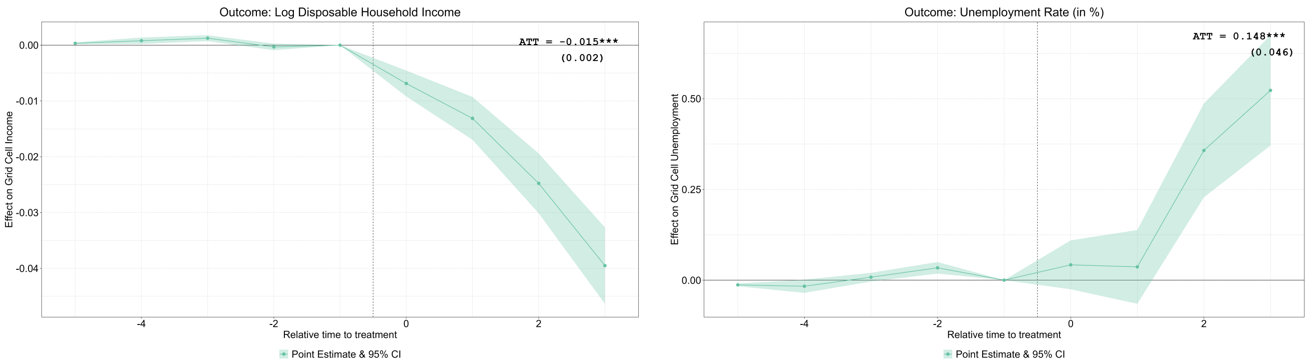

(a) Disposable Household Income (in logs)

(b) Unemployment Rate

Note: The figure shows point estimates and 95% confidence intervals for θ_s from Equation (2). The outcome variables are the natural logarithm of disposable household income per adult (Panel (a)) and the unemployment rate (Panel (b)) at the grid cell level. The sample consists of all grid cells within a 10 km radius around plants that close down during the sample period. Standard errors are clustered by municipality. The ATT estimates in the top right corner of each panel represent the joint effect across all post-treatment periods.

Figure B.5: Effect of IRD Closure on Disposable Household Income and Unemployment – Heterogeneity by Baseline Industrial Employment Share

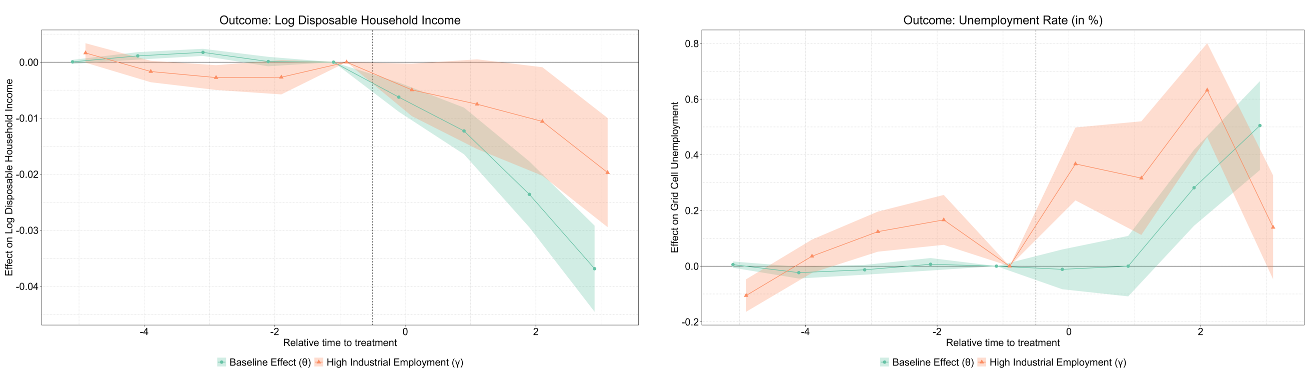

(a) Household Income (in logs)

(b) Unemployment

Note: The figure shows point estimates and 95% confidence intervals for θ_s and γ_s from Equation (3). The outcome variables are the natural logarithm of disposable household income per adult (Panel (a)) and the unemployment rate (Panel (b)) at the grid cell level. The sample consists of all grid cells within a 10 km radius around plants that close down during the sample period. Standard errors are clustered by municipality.

Figure B.6: Effect of IRD Closure on Air Quality

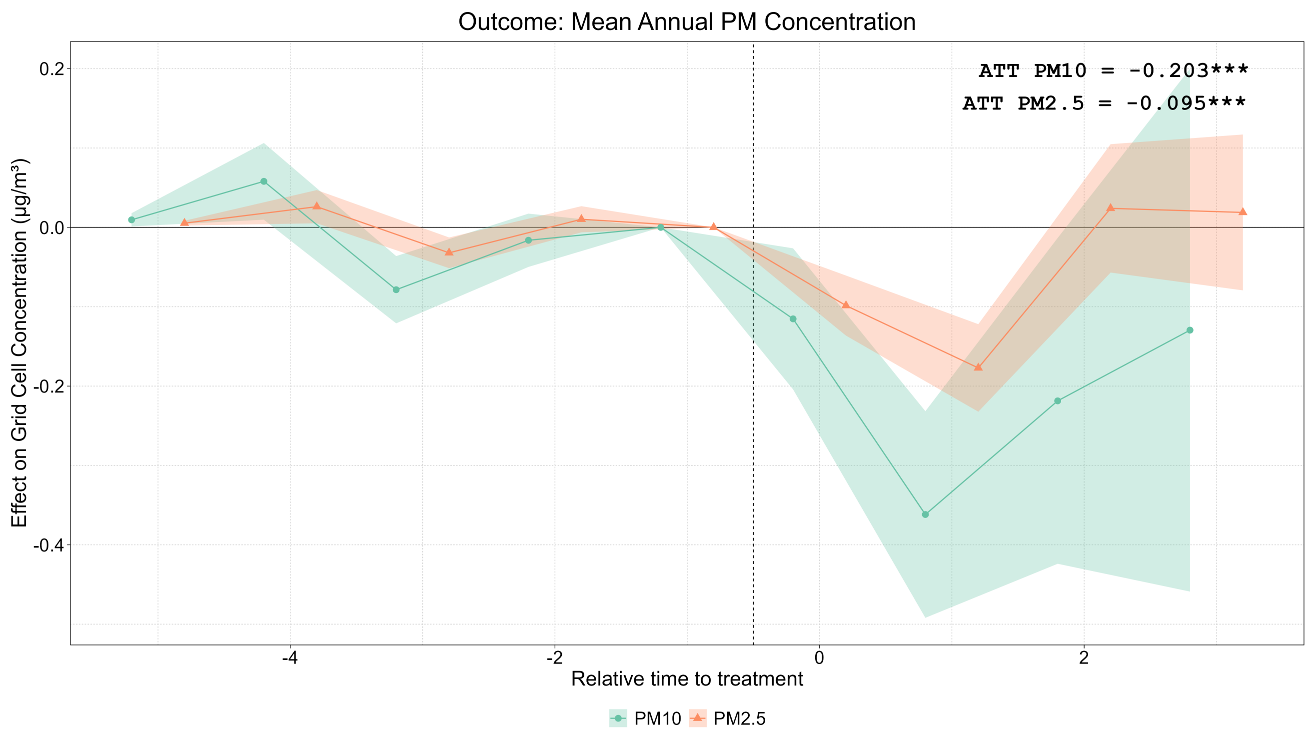

Note: The figure shows point estimates and 95% confidence intervals for θ_s from Equation (2). The outcome variable is the mean annual PM2.5 or PM10 concentration at the grid cell level as measured by van Donkelaar et al. (2021) and Umweltbundesamt (2023) respectively. Controls include mean temperature, average daily precipitation and the magnitude of the mean wind vector. The sample consists of all grid cells within a 10 km radius around plants that close down during the sample period and that fall within a single treatment buffer. Standard errors are clustered by municipality. The ATT estimates in the top right corner represent the joint effect across all post-treatment periods.

Figure B.7: Effect of IRD Closure on Adult Population (in logs)

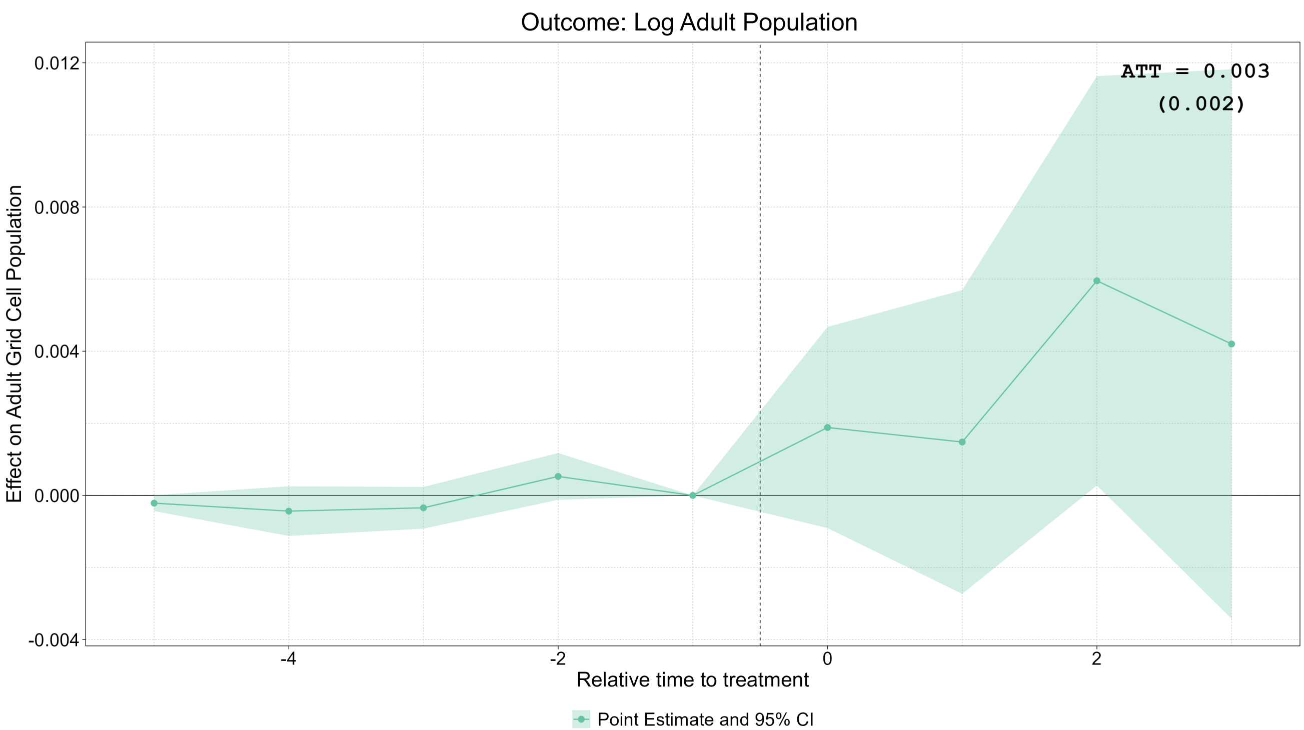

Note: The figure shows point estimates and 95% confidence intervals for θ_s from Equation (2). The outcome variable is the natural logarithm of adult population at the grid cell level. The sample consists of all grid cells within a 10 km radius around plants that close down during the sample period. Standard errors are clustered by municipality. The ATT estimate in the top right corner represents the joint effect across all post-treatment periods.

C ROBUSTNESS CHECKS – 2KM BUFFER

Table C.1: Effect of IRD Closure on Air Quality

Dependent Variables:	PM2.5 (van Donkelaar)				PM10 (UBA)			
Model:	(1)	(2)	(3)	(4)	(5)	(6)	(7)	(8)
Closure	-0.0474	-0.0461	-0.0578*	-0.0597	-0.2124**	-0.2130**	-0.2724***	-0.2193*
	(0.0362)	(0.0316)	(0.0343)	(0.0365)	(0.1000)	(0.0973)	(0.0942)	(0.1195)
Single Treatment			✓				✓	
Weather Controls		✓	✓	✓		✓	✓	✓
Year	✓	✓	✓		✓	✓	✓	
Year × Sector				✓				✓
Grid Cell	✓	✓	✓	✓	✓	✓	✓	✓
Observations	49,276	49,276	42,612	41,347	49,220	49,220	42,584	41,302
R^2	0.00134	0.00141	0.00217	0.00275	0.00455	0.00470	0.00773	0.00536
Adjusted R^2	0.00134	0.00141	0.00217	0.00275	0.00455	0.00470	0.00773	0.00536

Clustered standard errors (Municipality) in parentheses.
*Signif. Codes: ***: 0.01, **: 0.05, *: 0.1*

Note: The table shows ATT estimates for the effect of IRD closures on mean annual particulate matter concentration across all post-treatment periods for grid cells located within 2km of a closing IRD plant. Columns (1) - (4) report results for PM2.5 provided by van Donkelaar et al. (2021) and columns (5) - (8) report results for PM10 from Umweltbundesamt (2023). Columns (3) and (7) exclude grid cells located within 2km of multiple closing plants. Reduced sample size in columns (4) and (8) is due to incomplete sector assignments at the facility level. Standard errors are clustered by municipality.

Table C.2: Effect of IRD Closure on Neighborhood Amenities

Dependent Variable:	Log Amenity Index		
Housing share parameter:	$\alpha = 0.2$	$\alpha = 0.3$	$\alpha = 0.4$
Panel A: Low Mobility Elasticity ($\phi = 2$)			
Closure	0.0022	0.0037	0.0051
	(0.0056)	(0.0064)	(0.0073)
Closure × Industrial	-0.0160**	-0.0254***	-0.0349***
	(0.0077)	(0.0091)	(0.0107)
Panel B: Baseline Mobility Elasticity ($\phi = 4.56$)			
Closure	0.0018	0.0033	0.0048
	(0.0051)	(0.0059)	(0.0068)
Closure × Industrial	-0.0105*	-0.0199***	-0.0294***
	(0.0063)	(0.0076)	(0.0091)
Panel C: High Mobility Elasticity ($\phi = 6$)			
Closure	0.0018	0.0032	0.0047
	(0.0050)	(0.0058)	(0.0068)
Closure × Industrial	-0.0094	-0.0189**	-0.0284***
	(0.0061)	(0.0073)	(0.0089)
Fixed Effects			
Year	✓	✓	✓
Grid Cell	✓	✓	✓
Observations	28,477	28,477	28,477

Clustered standard errors (Municipality) in parentheses.
*Signif. Codes: ***: 0.01, **: 0.05, *: 0.1*

Note: The table displays ATT estimates across all post-treatment periods for the effect of IRD closures on local amenities (in logs) as specified in Equation (9). The different panels display results for varying values of ϕ and columns show results for varying values of α. Amenities are computed as in Equation (8). The sample includes all grid cells within a 2km radius of closing IRD sites that have recorded house listings. Standard errors are clustered by municipality.

Table C.3: Effect of IRD Closure on House Prices and Apartment Rents

Dependent Variables:	House Prices			Apartment Rents		
Model:	(1)	(2)	(3)	(4)	(5)	(6)
Closure	0.0023	0.0067	-0.0065	-0.0020	-0.0003	-0.0053
	(0.0123)	(0.0133)	(0.0128)	(0.0073)	(0.0076)	(0.0080)
Single Treatment		✓			✓	
Year	✓	✓		✓	✓	
Year × Sector			✓			✓
Grid Cell	✓	✓	✓	✓	✓	✓
Observations	28,656	24,145	24,261	27,682	22,835	23,577
R^2	-2.5×10^{-5}	3.92×10^{-5}	4.59×10^{-5}	1.75×10^{-5}	-4.26×10^{-5}	0.00035
Adjusted R^2	-2.5×10^{-5}	3.92×10^{-5}	4.59×10^{-5}	1.75×10^{-5}	-4.26×10^{-5}	0.00035

Clustered standard errors (Municipality) in parentheses.
*Signif. Codes: ***: 0.01, **: 0.05, *: 0.1*

Note: The table shows ATT estimates for the effect of IRD closures on mean house prices (Columns (1) - (3)) and apartment rents (Columns (4) - (6)) at the grid cell level. Columns (1) and (4) show the effects for the full sample, i.e. all grid cells located within a 2km radius of a closing plant. Columns (2) and (5) show the results from a specification excluding grid cells located within 2km of *multiple* closing plants. Columns (3) and (6) show the results from a specification including sector-by-year fixed effects. Standard errors are clustered by municipality. Varying sample sizes are due to some grid cells not having any recorded listings in certain years.

Table C.4: Effect of IRD Closure on Disposable Household Income and Unemployment

Dependent Variables:	Income				Unemployment			
Model:	(1)	(2)	(3)	(4)	(5)	(6)	(7)	(8)
Closure	-0.0056*	-0.0039	-0.0032	-0.0050	-0.0347	-0.1197	-0.1592*	-0.0895
	(0.0033)	(0.0034)	(0.0037)	(0.0037)	(0.0895)	(0.0927)	(0.0961)	(0.0958)
Closure × Industrial		-0.0114**	-0.0078	-0.0125**		0.6591***	0.5845***	0.7379***
		(0.0052)	(0.0048)	(0.0056)		(0.1776)	(0.1927)	(0.1309)
Single Treatment			✓				✓	
Year	✓	✓	✓		✓	✓	✓	
Year × Sector				✓				✓
Grid Cell	✓	✓	✓	✓	✓	✓	✓	✓
Observations	49,276	48,869	42,443	41,020	49,276	48,869	42,443	41,020
R^2	0.00304	0.00513	0.00258	0.00728	0.00018	0.01137	0.00900	0.01571
Adjusted R^2	0.00304	0.00511	0.00255	0.00726	0.00018	0.01135	0.00898	0.01568

Clustered standard errors (Municipality) in parentheses.
*Signif. Codes: ***: 0.01, **: 0.05, *: 0.1*

Note: The table shows ATT estimates for the effect of IRD closures on log disposable household income per adult (Columns (1) - (4)) and the unemployment rate (Columns (5) - (8)) at the grid cell level. The first column for each outcome shows the aggregate treatment effect for both variables, the second column for each outcome shows the baseline effect and the interaction effect for grid cells with high baseline industrial employment. The third column for each outcome shows the results from a specification excluding grid cells located within 2km of multiple closing plants. The fourth column for each outcome shows the results from a specification with sector-by-year fixed effects. Standard errors are clustered by municipality.

Figure C.1: Pre-Treatment Evolution of Outcomes across Treatment Cohorts

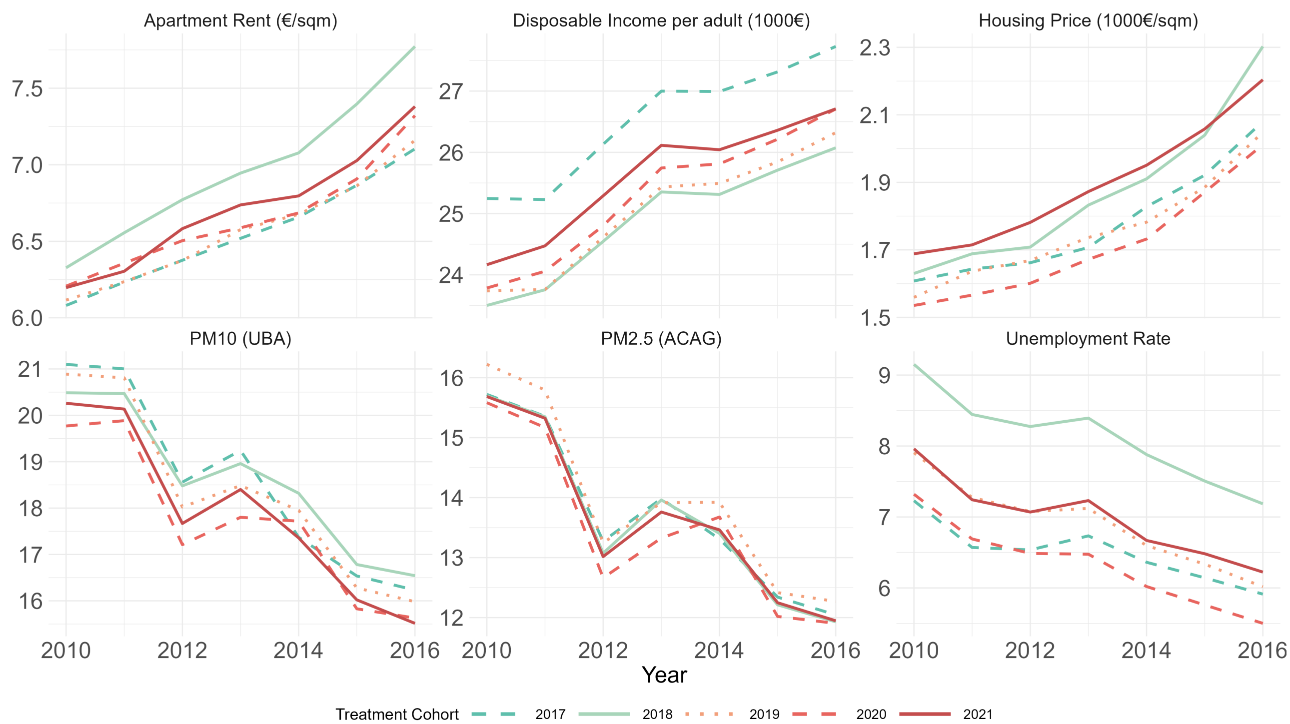

Note: The figure shows the evolution of all outcome variables used in the event study specification of Equation (2) over the common pre-treatment period 2010–2016, separately by treatment cohort. Cohorts are defined by the year of the first IRD closure affecting a given grid cell. Lines represent unweighted averages across all grid cells in a given cohort. The sample is restricted to grid cells within 2 km of a closing IRD plant. PM2.5 (ACAG) refers to the satellite-based pollution measures by van Donkelaar et al. (2021). PM10 (UBA) refers to the monitor-based measure from Umweltbundesamt (2023).

Figure C.2: Treatment Effect Heterogeneity for PM2.5 by Income Decile

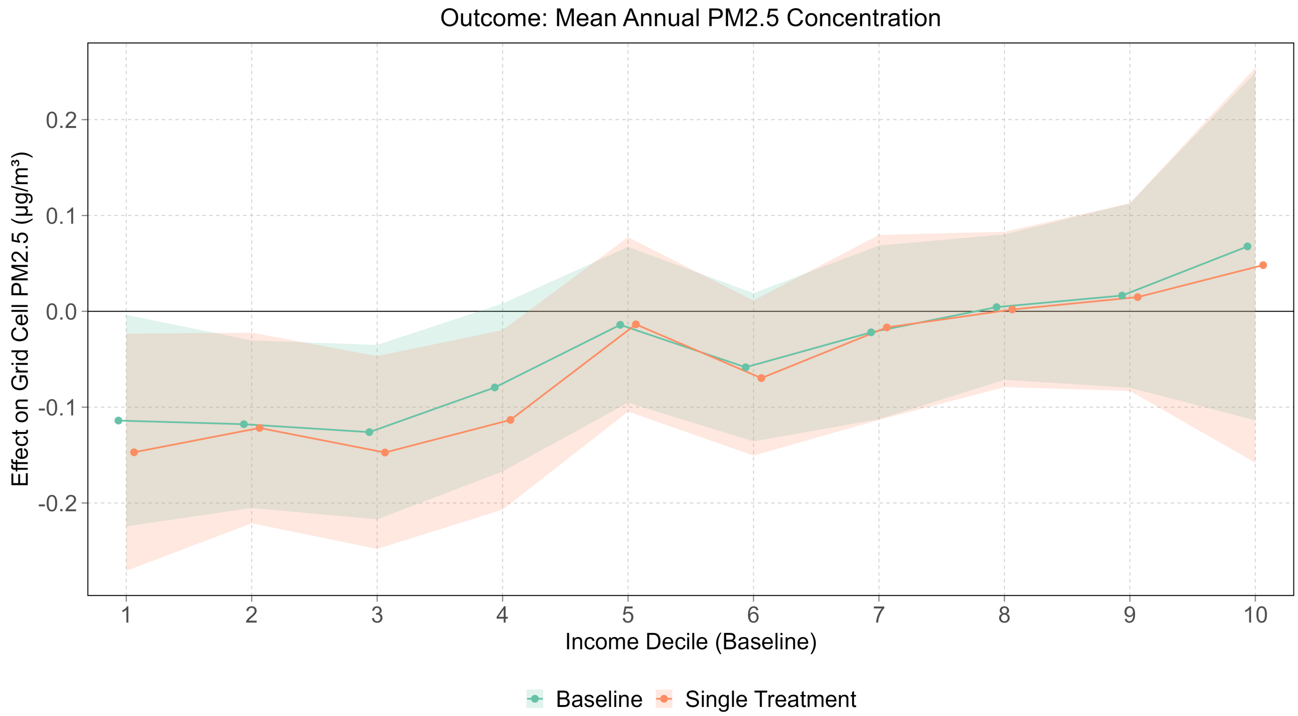

Note: The figure shows the average treatment effect and 95% confidence interval for the effect of an IRD shutdown on PM2.5 concentration in surrounding grid cells averaged across all post-treatment periods by baseline (pre-treatment) income decile of the treated grid cells. Estimates correspond to results obtained using the model from Equation (2) with treatment interacted with baseline income decile. Standard errors are clustered by municipality. Single Treatment refers to estimates obtained excluding grid cells located in the intersection of multiple treatment buffers.

Figure C.3: Effect of IRD Closure on House Prices and Apartment Rents

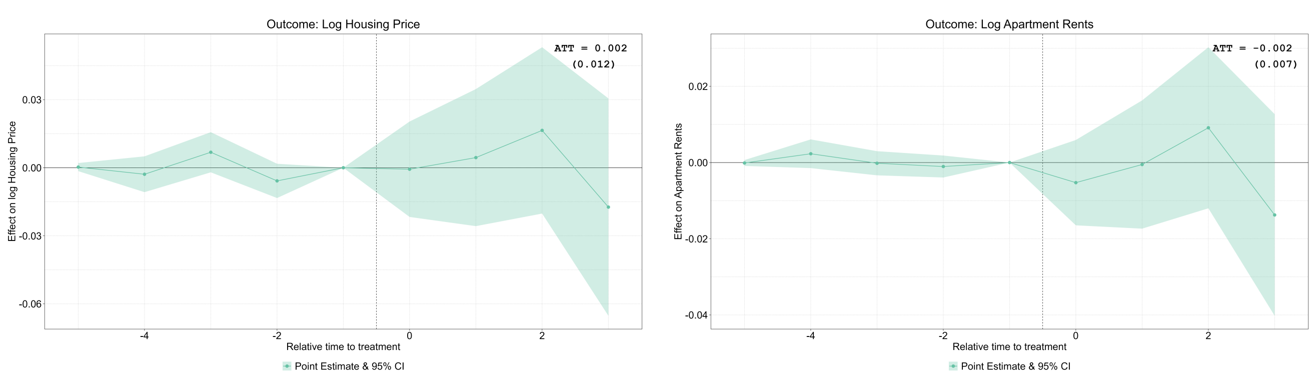

(a) House Prices (in logs)

(b) Apartment Rents (in logs)

Note: The figure shows point estimates and 95% confidence intervals for θ_s from Equation (2). The outcome variables are the natural logarithm of average house prices per square meter (Panel (a)) and average apartment rents per square meter (Panel (b)) at the grid cell level. The sample consists of all grid cells within a 2 km radius around plants that close down during the sample period. Standard errors are clustered by municipality. The ATT estimates in the top right corner of each panel represent the joint effect across all post-treatment periods.

Figure C.4: Effect of IRD Closure on Disposable Household Income and Unemployment

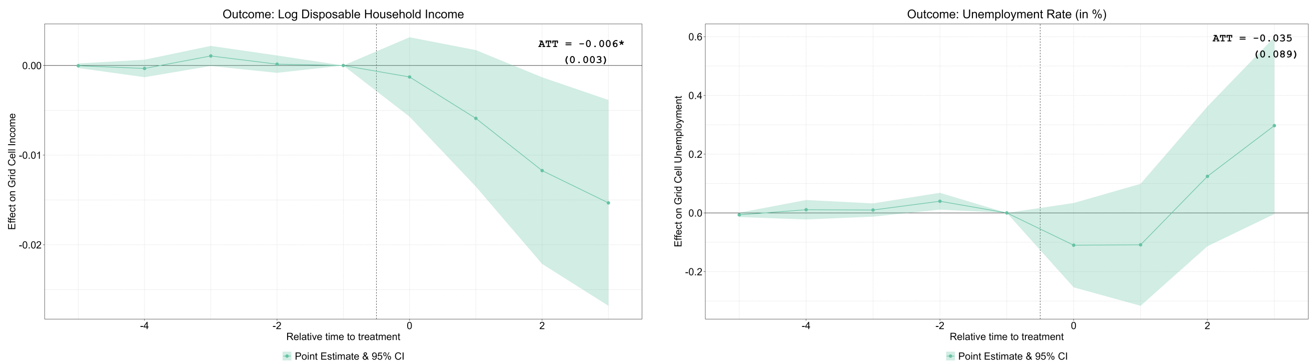

(a) Disposable Household Income (in logs)

(b) Unemployment

Note: The figure shows point estimates and 95% confidence intervals for θ_s from Equation (2). The outcome variables are the natural logarithm of disposable household income per adult (Panel (a)) and the unemployment rate (Panel (b)) at the grid cell level. The sample consists of all grid cells within a 2 km radius around plants that close down during the sample period. Standard errors are clustered by municipality. The ATT estimates in the top right corner of each panel represent the joint effect across all post-treatment periods.

Figure C.5: Effect of IRD Closure on Disposable Household Income and Unemployment — Heterogeneity by Baseline Industrial Employment Share

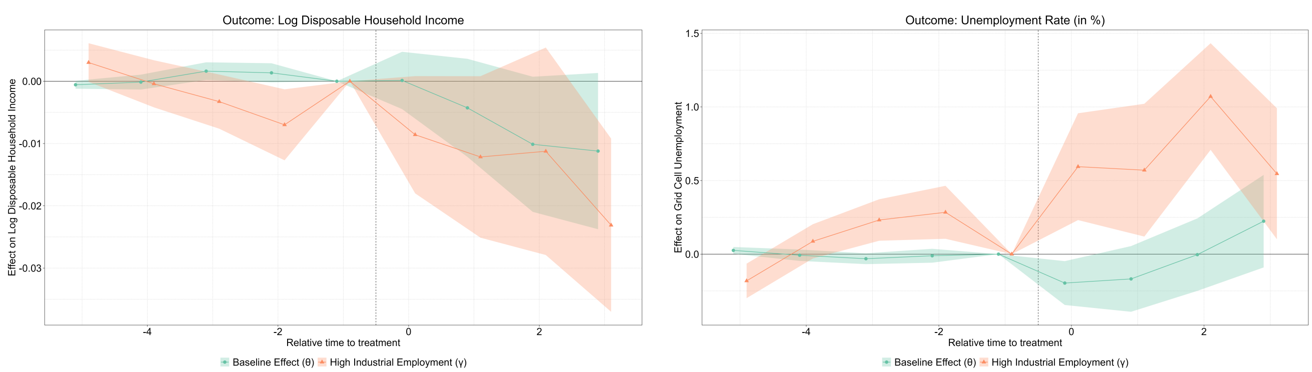

(a) Disposable Household Income (in logs)

(b) Unemployment

Note: The figure shows point estimates and 95% confidence intervals for θ_s and γ_s from Equation (3). The outcome variables are the natural logarithm of disposable household income per adult (Panel (a)) and the unemployment rate (Panel (b)) at the grid cell level. The sample consists of all grid cells within a 2 km radius around plants that close down during the sample period. Standard errors are clustered by municipality.

Figure C.6: Effect of IRD Closure on Air Quality

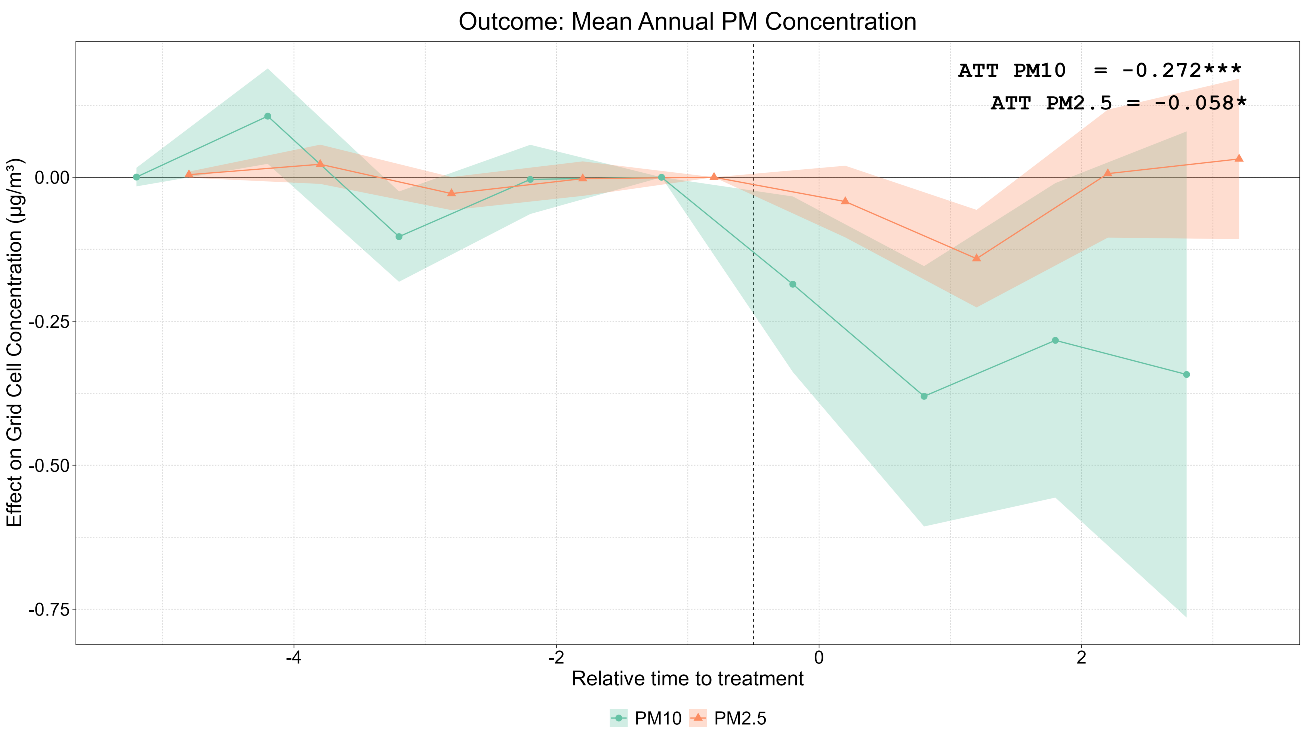

Note: The figure shows point estimates and 95% confidence intervals for θ_s from Equation (2). The outcome variable is the mean annual PM2.5 or PM10 concentration at the grid cell level as measured by van Donkelaar et al. (2021) and Umweltbundesamt (2023) respectively. Controls include mean temperature, average daily precipitation and the magnitude of the mean wind vector. The sample consists of all grid cells within a 2 km radius around plants that close down during the sample period and that fall within a single treatment buffer. Standard errors are clustered by municipality. The ATT estimates in the top right corner represent the joint effect across all post-treatment periods.

Figure C.7: Effect of IRD Closure on Adult Population (in logs)

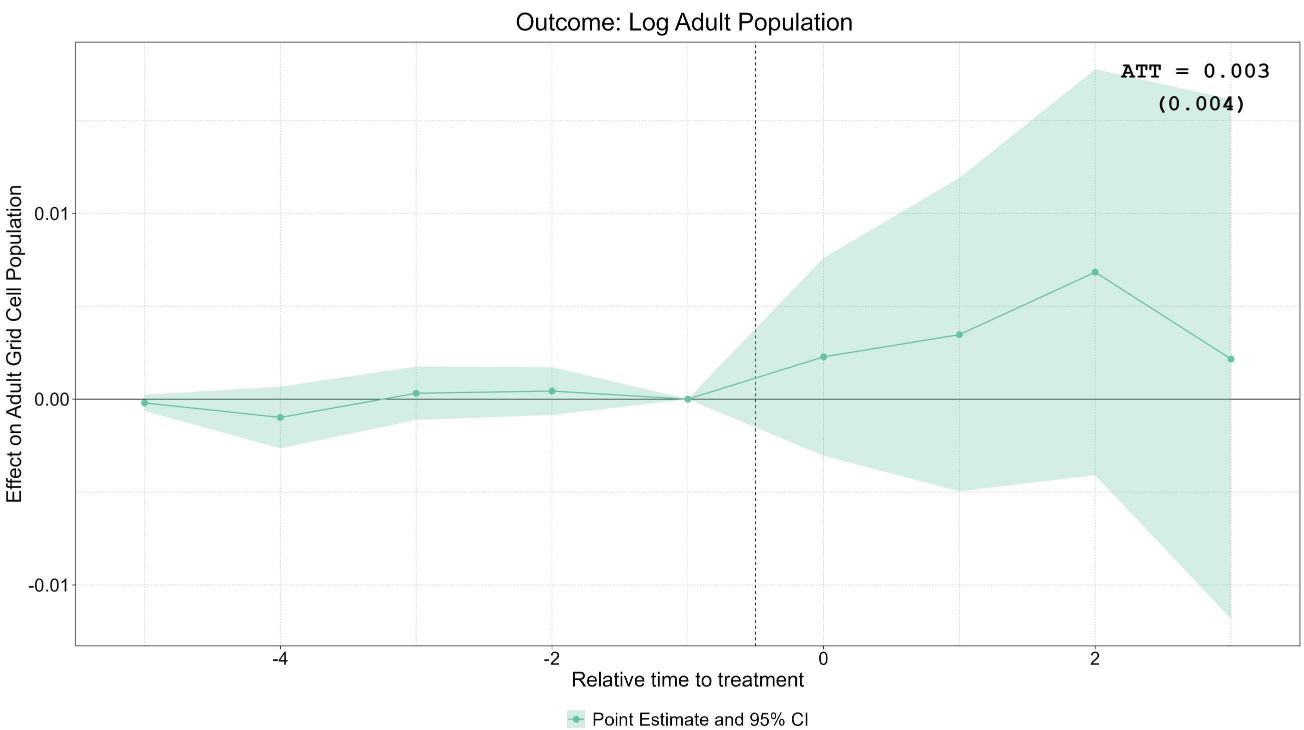

Note: The figure shows point estimates and 95% confidence intervals for θ_s from Equation (2). The outcome variable is the natural logarithm of adult population at the grid cell level. The sample consists of all grid cells within a 2 km radius around plants that close down during the sample period. Standard errors are clustered by municipality. The ATT estimate in the top right corner represents the joint effect across all post-treatment periods.

D ROBUSTNESS CHECKS – GROUP-SPECIFIC TIME EFFECTS

The model specified in Equation (3) absorbs common time effects, ω_t, across districts with and without high baseline industrial employment shares. Implicitly, this postulates common trends across the two types of districts in the absence of a closure. The interaction effect is thus identified off comparisons between treated high industrial employment cells and not-yet-treated high and low industrial employment cells alike. Given the non-zero pre-treatment coefficients in the unemployment panel of Figure 5, a legitimate concern is that the interaction effect spuriously attributes a closure effect to differential outcome trends in the set of highly industrialized grid cells. To mitigate this concern, I re-estimate the closure penalty while allowing for differential time effects across the two groups of grid cells

$$Y_{nt} = \sum_{s \neq -1} (\theta_s + \gamma_s \text{IndEmpl}_n) \cdot \mathbb{1}[t - \tau_n = s] + \mu_n + \omega_{IndEmpl \times t} + \epsilon_{nt} \tag{17}$$

This specification exactly mirrors Equation (3) with the exception of estimating the baseline and interaction treatment effects only relative to the subset of not-yet-treated grid cells *within the same partition of grid cells* defined by their baseline industrial employment shares. The results displayed in Figure D.1 show that the pre-trends in Figure 5 are attributable to differential time trends between the two groups of districts. Reassuringly, both the baseline and interaction effects remain qualitatively unchanged when absorbing year effects for both groups separately. This result shows that the unemployment effects in the main specification are not an artifact of differential group trends but represent genuine closure impacts.

Figure D.1: Effect of IRD Closure on Disposable Household Income and Unemployment – Heterogeneity by Baseline Industrial Employment Share

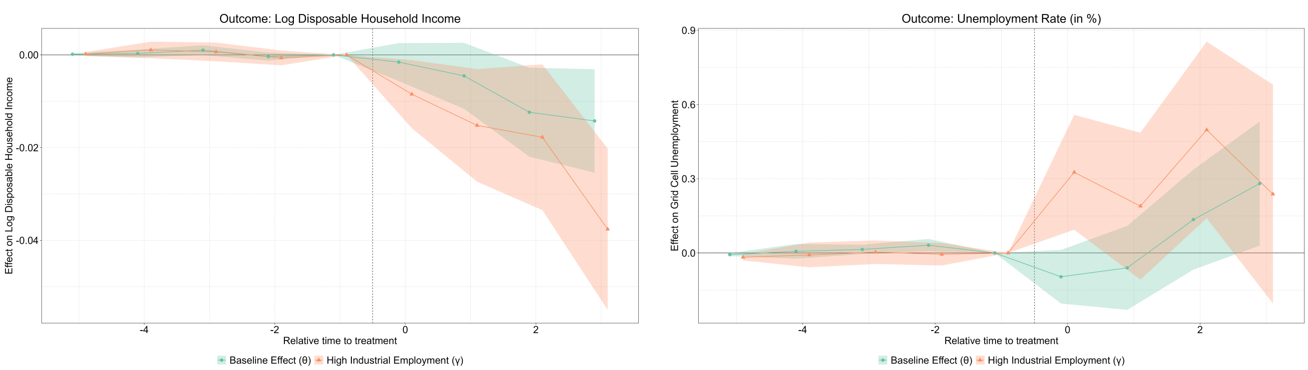

(a) Disposable Household Income (in logs)

(b) Unemployment Rate

Note: The figure shows point estimates and 95% confidence intervals for θ_s and γ_s from Equation (17). The outcome variables are the natural logarithm of average disposable household income per adult (Panel (a)) and the unemployment rate (Panel (b)) at the grid cell level. The sample consists of all grid cells within a 5 km radius around plants that close down during the sample period. Standard errors are clustered by municipality.

E ROBUSTNESS CHECKS – DISTANCE-RING SPECIFICATION FOR POLLUTION DECAY

The baseline specification defines treatment as a binary indicator equal to one for all grid cells within a contiguous radius of a closing plant. This definition implicitly assumes that the air quality impact of a closure does not decay so sharply with distance that pooling all cells within the buffer averages a large effect in the immediate vicinity of the plant with a negligible effect at the buffer's edge. To assess this assumption, I partition the 10km buffer around each closing facility into five mutually exclusive 2km distance rings and estimate ring-specific treatment effects in a single regression:

$$Y_{nt} = \sum_{r=1}^{5} \delta_r \cdot \mathbb{1}[t \geq \tau_n] \cdot \mathbb{1}[R_n = r] + C_{nt}\beta + \mu_n + \omega_t + \epsilon_{nt} \tag{18}$$

where $\mathbb{1}[t \geq \tau_n]$ indicates years following the closure that treats grid cell n and R_n assigns grid cell n to one of five distance rings (0–2km, 2–4km, 4–6km, 6–8km, 8–10km) based on the distance between the cell centroid and the closing facility. All other terms are defined as in Equation (2), and estimation again relies on the two-stage estimator of Gardner et al. (2024). Note that no ring serves as the omitted category: each δ_r measures the average post-closure effect for treated cells in ring r relative to the not-yet-treated counterfactual, so the five coefficients are directly comparable ring-specific ATTs.

The sample used to estimate the distance profile is restricted to grid cells exposed to a single closure during the observation window to avoid contamination from additional closures within different ring radii. Also note that the specification imposes common year fixed effects across rings rather than ring-specific time effects. Each δ_r is therefore identified, as in the baseline design, from the comparison of treated cells in ring r to not-yet-treated cells; but because all rings around a given facility enter treatment in the same year, the composition of treatment cohorts is identical across rings by construction, and differences between the ring coefficients reflect near-versus-far contrasts within closure events rather than differences in closure timing or cohort composition across rings.

Figure E.1 reports the ring-specific ATTs for both pollution measures. Within a radius of 10km, the estimated effects display no discernible decay in distance to the closing plant. For PM2.5, the ring-specific ATTs range between -0.08 and -0.11 $\mu g/m^3$, with the largest point estimate in the 6–8km ring; for PM10, they range between -0.16 and -0.23 $\mu g/m^3$, with the largest point estimate in the outermost ring. In neither case do the estimates significantly decline in magnitude with distance.

The approximately uniform spatial profile supports the treatment definition used throughout the paper: within the buffers considered, a binary contiguous-buffer indicator captures the relevant variation, and the estimated pollution response is not an artifact of averaging a strong near-source effect with null effects at the periphery of the buffer. The absence of decay is unsurprising given the narrow spatial window: the entire 10km study area is small relative to the distances over which closure effects have been documented. For instance, Fraenkel et al. (2024) find housing price effects of coal unit retirements within 15 miles ($\approx$ 24km) of the closing plant and emissions from elevated stacks attain their maximum ground-level concentration several kilometers downwind of the source rather than at the plant boundary. Note, however, that unlike Fraenkel et al. (2024) and Currie et al. (2015), who identify effects from comparisons of near versus far locations around the same site, the design in this paper retains the staggered-timing counterfactual of the baseline specification throughout: treated cells are compared to not-yet-treated cells, and the rings serve only to trace out the spatial profile of the effect.

Figure E.1: Effect of IRD Closure on Particulate Matter Concentration by Distance to Closing Plant

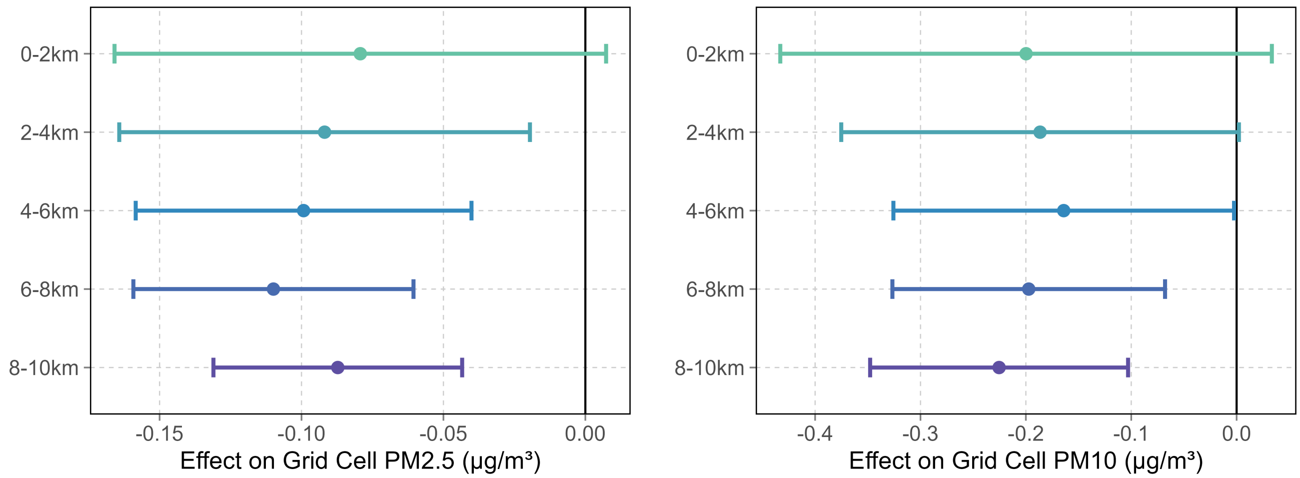

(a) PM2.5

(b) PM10

Note: The figure shows ATT estimates and 95% confidence intervals for δ_r from Equation (18). The outcomes are mean annual PM2.5 concentration as measured by van Donkelaar et al. (2021) (Panel (a)) and mean annual PM10 concentration from Umweltbundesamt (2023) (Panel (b)) at the grid cell level. Distance rings are measured from the grid cell centroid to the facility whose closure defines the cell's treatment date. The sample consists of all grid cells within a 10km radius of a closing IRD plant that are exposed to a single closure during the sample period. Controls include average annual temperature, average daily precipitation, and the magnitude of the mean wind vector. Standard errors are clustered by municipality.

F ROBUSTNESS CHECKS – PROPERTY-LEVEL ESTIMATES FOR HOUSING PRICES AND APARTMENT RENTS

The results shown in Figure 3 display the effect of IRD closures on mean housing prices and apartment rents at the grid cell level. A potential concern with collapsing listings to grid cell averages is that IRD closures might be correlated with changes in the composition of properties listed for sale or rent. In that case, the estimated treatment effects would partly capture compositional shifts rather than valuation changes for a given bundle of property characteristics.

To address this concern, I report a property-level variant of the main specification below. Estimating treatment effects at the property level allows me to control directly for observable property characteristics and is therefore less susceptible to compositional bias, although such bias may still arise along unobserved dimensions. Concretely, I estimate the property-level analog of Equation (3):

$$y_{pnt} = \sum_{s \neq -1} (\theta_s + \gamma_s \text{IndEmpl}_n) \cdot \mathbb{1}[t - \tau_n = s] + X_{pt}\zeta + \mu_n + \omega_t + \epsilon_{pnt} \tag{19}$$

where y_{pnt} denotes the log listing price (rent) for house (apartment) p located in grid cell n in year t. X_{pt} is a vector of property-level controls. For houses, these comprise the natural logarithms of living area and plot size (both in m^2), along with dummies for the number of rooms and the year of construction. For apartments, controls include log living area and dummies for the number of rooms, year of construction, and floor. For listings that appear in consecutive years, I retain only the latest entry, as it is the most likely to reflect the final transaction price. Since most properties consequently appear in the data only once, I retain grid-cell fixed effects and control for observable property characteristics rather than adopting a repeat sales framework. Standard errors are clustered at the municipality level.

Table F.1 reports the corresponding static treatment effects. The aggregate ATTs in columns (1) and (5) indicate drops of 1.5% and 0.9% in listing prices and rents respectively, producing point estimates strikingly close to the grid-cell aggregates, though neither is statistically significant at conventional levels. Allowing the effect to vary by baseline industrial employment (columns (2) and (6)) reproduces the expected pattern of heterogeneity: in highly industrial areas, listing prices fall by 8.6% more than in non-industrial regions, where prices do not respond significantly. A similar pattern emerges for apartment rents, with an additional 4% reduction in industrial areas. The pattern is robust to restricting the sample to grid cells exposed to a single closure (columns (3) and (7)) and to the inclusion of sector-by-year fixed effects (columns (4) and (8)). Figure F.1 plots the corresponding event study coefficients, underscoring the substantially larger magnitude of the price drop in highly industrial areas. Housing prices appear to rebound three years post-closure, but this estimate should be interpreted with caution as no analogous rebound is observed for rents, and effects at later horizons are estimated based on fewer control cohorts and are thus noisier.

Table F.1: Effect of IRD Closure on Housing Prices and Apartment Rents – Property Level

Dependent Variables:	Log Housing Price				Log Apartment Rent			
Model:	(1)	(2)	(3)	(4)	(5)	(6)	(7)	(8)
Closure	-0.0150	-0.0066	-0.0113	-0.0186*	-0.0086	-0.0064	-0.0079	-0.0137
	(0.0106)	(0.0107)	(0.0119)	(0.0110)	(0.0104)	(0.0106)	(0.0097)	(0.0115)
Closure × Industrial		-0.0861***	-0.0496*	-0.0719***		-0.0404**	-0.0453**	-0.0439**
		(0.0230)	(0.0291)	(0.0265)		(0.0164)	(0.0228)	(0.0213)
Single Treatment			✓				✓	
Year	✓	✓	✓		✓	✓	✓	
Year × Sector				✓				✓
Grid Cell	✓	✓	✓	✓	✓	✓	✓	✓
Observations	706,282	706,282	469,434	623,759	2,069,019	2,069,019	1,144,404	1,777,883
R^2	0.00036	0.00157	0.00059	0.00198	0.00040	0.00096	0.00105	0.00205
Adjusted R^2	0.00036	0.00157	0.00059	0.00198	0.00040	0.00096	0.00105	0.00205

Clustered standard errors (Municipality) in parentheses.
*Signif. Codes: ***: 0.01, **: 0.05, *: 0.1*

Note: The table shows ATT estimates for the effect of IRD closures on the natural logarithm of the listed sale price per house (Columns (1) - (4)) and the cold rent per apartment (Columns (5) - (8)) at the property level. The first column for each outcome shows the aggregate treatment effect for both variables, the second column for each outcome shows the baseline effect and the interaction effect for properties located in areas with high baseline industrial employment. The third column for each outcome shows the results from a specification excluding grid cells located within 5km of multiple closing plants. The fourth column for each outcome shows the results from a specification with sector-by-year fixed effects. Hedonic controls include log living area, log plot area (houses only), and fixed effects for number of rooms and construction year and for apartment floor (apartments only). Standard errors are clustered by municipality.

Figure F.1: Effect of IRD Closure on Housing Prices and Apartment Rents – Property Level

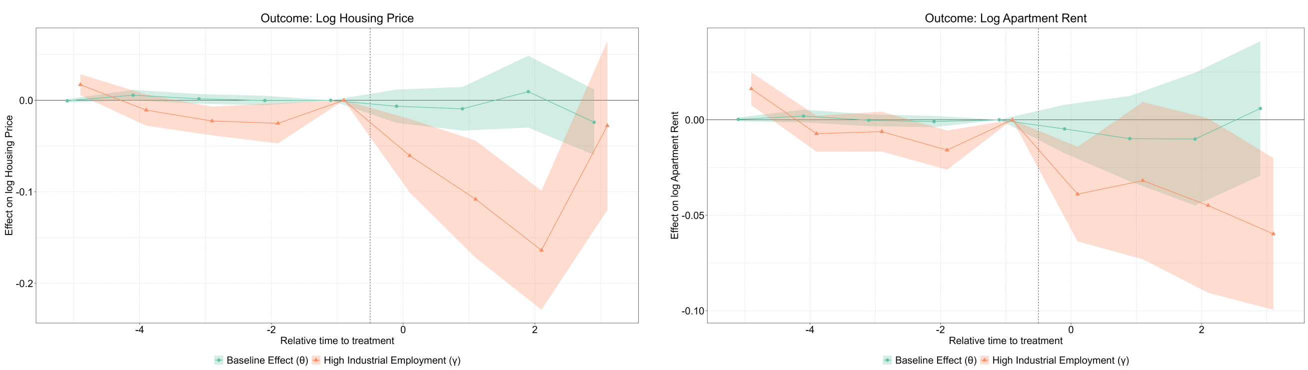

(a) House Prices (in logs)

(b) Apartment Rents (in logs)

Note: The figure shows point estimates and 95% confidence intervals for θ_s and γ_s from Equation (19). The outcome variables are the natural logarithm of the listed sale price per house (Panel (a)) and the cold rent per apartment (Panel (b)). The sample consists of all individual properties within a 5 km radius around plants that close down during the sample period. Standard errors are clustered by municipality.